**Proper chromosome alignment depends on BRCA2 phosphorylation by PLK1**

Åsa Ehlén[1,2], Charlotte Martin[1,2†], Simona Miron[3†], Manon Julien[3,4†], François-Xavier Theillet[3], Virginie Boucherit[1,2], Virginie Ropars[3], Patricia Duchambon[5,6], Ahmed El Marjou[5,7], Sophie Zinn-Justin[3*], Aura Carreira[1,2, 8,*,#]

[1]Institut Curie, PSL Research University, CNRS, UMR3348, F-91405, Orsay, France

[2]Paris Sud University, Paris-Saclay University CNRS, UMR3348, F-91405 Orsay, France

[3]Institute for Integrative Biology of the Cell (I2BC), CEA, CNRS, Univ Paris-Sud, Université Paris-Saclay, Gif-sur-Yvette Cedex, France

[4]Department of Biology, École Normale Supérieure, 94230 Cachan, France
[5]Protein Expression and Purification Core Facility, Institut Curie, 26 rue d'Ulm, 75248 Paris Cedex 05, France
[6]INSERM U1196, 91405 Orsay Cedex, France
[7]CNRS UMR144, 12 rue Lhomond, 75005 Paris, France
[8]Lead contact

[†] Equal contributors
[*] co-corresponding authors

[#]To whom correspondence should be addressed:
Aura Carreira
Institut Curie - Research Center
UMR 3348 CNRS "Genotoxic Stress and Cancer"
Bâtiment 110, Centre Universitaire
91405 Orsay
France
Phone: +33 (0)1 69 86 30 82
Fax: +33 (0)1 69 86 94 29
E-mail: aura.carreira@curie.fr

**Summary**

The BRCA2 tumor suppressor protein is involved in the maintenance of genome integrity through its role in homologous recombination. In mitosis, BRCA2 is phosphorylated by Polo-like kinase 1 (PLK1). Here we describe how this phosphorylation contributes to the control of mitosis. We identified two highly conserved phosphorylation sites at S193 and T207 of BRCA2. Phosphorylated-T207 is a bona fide docking site for PLK1 as illustrated by the crystal structure of the BRCA2 peptide bound to PLK1 Polo-box domain. We find that BRCA2 is in complex with PLK1, phosphorylated-BUBR1 and the phosphatase PP2A-B56α. Precluding BRCA2 binding to PLK1, as observed in *BRCA2* breast cancer variants, alters the tetrameric complex resulting in misaligned chromosomes, faulty chromosome segregation and aneuploidy. We thus reveal a direct role of BRCA2 in the alignment of chromosomes, distinct from its DNA repair function, with important consequences on chromosome stability. These findings may explain the aneuploidy observed in *BRCA2*-mutated tumors.

**Keywords**

BRCA2; chromosome alignment; variants of uncertain clinical significance (VUS); PLK1; phosphorylation; BUBR1; mitosis; chromosome instability; breast cancer

## Introduction

The BRCA2 tumor suppressor protein plays an important role in DNA repair by homologous recombination (HR)(Jensen et al., 2010; Moynahan et al., 2001) which takes place preferentially during S/G2 phases of the cell cycle(Saleh-Gohari and Helleday, 2004). BRCA2 has also emerging functions in mitosis, for example, it binds to the spindle assembly component BUBR1(Futamura et al., 2000), facilitating the acetylation/deacetylation of the latter(Choi et al., 2012; Park et al., 2017), the function of which is poorly understood. At the end of mitosis, BRCA2 localizes to the midbody and facilitates cell division by serving as a scaffold protein for the central spindle components(Daniels et al., 2004; Mondal et al., 2012; Takaoka et al., 2014). BRCA2 is a target of phosphorylation by PLK1 both in its N-terminal region(Lin et al., 2003) and in its central region(Lee et al., 2004), although the functional role of these phosphorylation events remains unclear.

PLK1 is a master regulator of the cell cycle, especially in mitosis(Barr et al., 2004; Zitouni et al., 2014). Among other functions, PLK1 phosphorylates BUBR1 at several residues including the tension-sensitive sites S676 (Elowe et al., 2007) and T680 (Suijkerbuijk et al., 2012) in prometaphase allowing the formation of stable kinetochore-microtubule attachments. This activity needs to be tightly regulated to ensure proper alignment of the chromosomes at the metaphase plate (Elowe et al., 2007; 2010; Zhang et al., 2016); in particular, Aurora B is an essential kinase that destabilizes erroneous kinetochore-microtubule interactions (Hauf et al., 2003). The phosphatase PP2A-B56$\alpha$ protects initial kinetochore-microtubule interactions from excessive destabilization by Aurora B (Foley et al., 2011) and this function is achieved through its interaction with BUBR1 phosphorylated at the Kinetochore

Attachment and Regulatory Domain (KARD) motif (including residues S676 and T680) (Suijkerbuijk et al., 2012). So, BUBR1, PLK1, Aurora B and PP2A-B56$\alpha$ are necessary for the formation of stable kinetochore-microtubule attachments.

PLK1 is recruited to specific targets via its Polo-box domain (PBD) (Elia et al., 2003a). PBD interacts with phosphosites characterized by the consensus motif S-[pS/pT]-P/X(Elia et al., 2003b). These phosphosites are provided by a priming phosphorylation event, usually mediated by CDK1 or other proline-directed kinases(Barr et al., 2004); however, there is also evidence that PLK1 itself might create docking sites ("self-priming") during cytokinesis (Kang et al., 2006; Neef et al., 2003).

Several BRCA2 sites corresponding to PLK1 consensus motifs have been identified as phosphorylated in mitosis, some of which belong to a cluster of predicted phosphosites located in BRCA2 N-terminus around residue S193 (Lin et al., 2003). We set out to investigate which of these sites are phosphorylated by PLK1, and to reveal whether these phosphorylation events play a role in the regulation of mitotic progression. Here, we demonstrate that phosphorylated T207 is a *bona fide* docking site for PLK1. By investigating the phenotype of BRCA2 missense variants that limit the phosphorylation of T207, we reveal an unexpected role of BRCA2 in the alignment of chromosomes at the metaphase plate. We demonstrate that phosphorylation of BRCA2 T207 promotes further phosphorylation by PLK1 of the kinetochore tension-sensitive sites of BUBR1. This, in turn, facilitates the interaction of BUBR1 with the phosphatase PP2A-B56$\alpha$ required to counter excessive Aurora B activity at the kinetochores(Suijkerbuijk et al., 2012). A defect in this function of BRCA2 leads to chromosome instability manifested in chromosome misalignment, chromosome segregation errors and aneuploidy.

## Results

### *BRCA2* variants identified in breast cancer reduce the PLK1-dependent phosphorylation of BRCA2 N-terminal region

Several missense variants of uncertain significance (VUS) identified in *BRCA2* in breast cancer patients are located in the N-terminal region predicted to be phosphorylated by PLK1 (around S193) (Breast information core (BIC)(Szabo et al., 2000) and BRCAshare (Béroud et al., 2016)), summarized in Table S1. To find out if any of these variants affect PLK1 phosphorylation in this region, we purified fragments comprising amino acids 1 to 250 of BRCA2 (hereafter $BRCA2_{1-250}$) from human embryonic kidney cells (HEK293T) and used an *in vitro* kinase assay to assess the phosphorylation by PLK1 of the fragments containing either the WT sequence, the different BRCA2 variants M192T, S196N, T200K, S206C and T207A, or the mutant S193A, previously reported to reduce the phosphorylation of BRCA2 by PLK1(Lin et al., 2003). As expected, S193A reduced the phosphorylation of $BRCA2_{1-250}$ by PLK1 (Figures 1A, 1B). Interestingly, variants T207A, S206C and T200K also led to a 2-fold decrease in PLK1 phosphorylation of $BRCA2_{1-250}$ (Figure 1A, 1B). In contrast, M192T slightly increased the phosphorylation above WT levels whereas VUS S196N did not significantly modify the phosphorylation of $BRCA2_{1-250}$ by PLK1 (Figure 1A, B). The phosphorylation observed in BRCA2 fragments is specific of the recombinant PLK1 kinase as replacing the WT PLK1 by a kinase-dead (PLK1-KD) version of the protein (K82R) (Golsteyn et al., 1995) purified using the same protocol, or adding a PLK1 inhibitor (BI3526) to the reaction, abolished the phosphorylation of $BRCA2_{1-250}$ (Figure 1C, lanes 4 and 5 compared to lane 3; Figure 1D). Moreover, running a kinase assay with $BRCA2_{1-250}$ alone did not result in any signal excluding a

kinase activity coming from a possible contaminant kinase in the preparation of $BRCA2_{1-250}$ produced in human cells, (Figure S1A, B).

Together, these results show that VUS T207A, S206C and T200K identified in breast cancer patients impair phosphorylation of $BRCA2_{1-250}$ by PLK1 *in vitro*.

**$BRCA2_{T207}$ is a target of phosphorylation by PLK1**

The reduction of BRCA2 phosphorylation in $BRCA2_{1-250}$ containing T207A and S206C variants suggested that T207 could be a target of PLK1 phosphorylation. We investigated this possibility by following the PLK1 phosphorylation kinetics of a truncated fragment of BRCA2 N-terminus comprising T207 (amino acids 190-283) (hereafter $BRCA2_{190-283}$) by Nuclear Magnetic Resonance (NMR) spectroscopy. NMR analysis allows residue-specific quantification of a peptide modification, provided it is $^{13}C$ or $^{15}N$-labelled. Figure 2A shows superimposed $^{1}H$-$^{15}N$ HSQC spectra of $BRCA2_{190-283}$ at different time points of the phosphorylation reaction with recombinant PLK1. Analysis of these experiments revealed phosphorylation of S193 and of eight other phosphosites, among which three threonines including T207 and five serines (Figure 2A). Four residues (T226>T207>T219>S193, Figure 2B, Figure S1C) were favoured phosphorylation sites, modified with markedly faster rates than the five other sites (S197, S217, S231, S239, S273). Interestingly, while T219 and T226 conservation is poor, T207 and S193 are conserved from mammals to fishes (Figures S1D and S1E) suggesting that both are important for BRCA2 function.

T207 phosphorylation together with the presence of a serine residue at position 206 creates a predicted docking site for $PLK1_{PBD}$(Elia et al., 2003b). Hence, we conclude that T207 is phosphorylated *in vitro* by PLK1, this phosphorylation is efficient in the context of $BRCA2_{190-283}$, and it may be a primary event for further BRCA2 phosphorylation via the recruitment of PLK1 to BRCA2.

**BRCA2 variants T207A and T200K alter the phosphorylation kinetics by PLK1**

Having identified T207 as a target of phosphorylation of PLK1, we next compared the residue-specific phosphorylation kinetics in the polypeptide WT $BRCA2_{190-283}$ containing the variants T207A or T200K that displayed reduced overall phosphorylation (Figure 1A, 1B). (The production of a $^{15}N$ recombinant fragment $BRCA2_{190-283}$ comprising S206C from bacteria yielded an insoluble protein precluding NMR analysis). Time-resolved NMR experiments revealed that PLK1 phosphorylates significantly less $BRCA2_{190-283}$ containing the variant T207A than the WT peptide (Figure 2C, 2D). Initial phosphorylation rates were decreased by a factor 5 (S193), 8 (T226) and 13 (T219) (Figure 2C, 2D, Figure S2A). Variant T200K reduced by half the phosphorylation rates of S193, T207, T219 and T226 (Figures 2E, 2F and Figure S2B).

In agreement with the *in vitro* kinase assay using the $BRCA2_{1-250}$ fragment purified from human cells (Figure 1), these results show that in $BRCA2_{190-283}$, variants T207A and T200K impair the phosphorylation of T207 and the cascade of associated phosphorylation events.

**Variants T207A, S206C and T200K reduce the interaction of BRCA2 and PLK1**

The finding that T207 is efficiently phosphorylated by PLK1 in $BRCA2_{190-283}$ polypeptide (Figure 2A) together with the observation that T207A mutation causes a global decrease in the phosphorylation of this region (Figure 2C) and the prediction that T207 is a docking site for $PLK1_{PBD}$ binding(Elia et al., 2003b) made us hypothesize that T207 might be a “self-priming” phosphorylation event required for the interaction of PLK1 with BRCA2 at this site. If so, the variants that reduce phosphorylation of T207 by PLK1 would be predicted to alter $PLK1_{PBD}$ binding. To

test this hypothesis, we examined the interaction of PLK1 with the VUS-containing polypeptides. We overexpressed 2xMBP-BRCA2$_{1-250}$ constructs carrying these variants in U2OS cells to detect the endogenous PLK1 that co-purifies with 2xMBP-BRCA2$_{1-250}$ using amylose pull-down. As expected, overexpressed BRCA2$_{1-250}$ was able to interact with endogenous PLK1 from mitotic cells but not from asynchronous cells (predominantly in G1/S) where the levels of PLK1 are reduced (Figure 3A, lane 2 compared to lane 1). As previously described (Lin et al., 2003), mutation S193A reduced the binding to PLK1 (Figure 3A, lane 6 compared to lane 2 and Figure 3B). Interestingly, the variants reducing PLK1 phosphorylation (T207A, S206C and T200K) showed a weaker interaction with PLK1 than the WT protein (Figure 3A, pull-down lane 4, 8 compared to lane 2 and lane 20 compared to lane 18, Figure 3B) despite the protein levels of PLK1 remaining unchanged (Figure 3A, compare PLK1 input lanes 4 and 8 to lane 2 and lane 20 to lane 18). In contrast, the effect of M192T and S196N on the interaction was mild (Figure 3A, compare pull-down lanes 12 and 14 to lane 10, Figure 3B). These results are consistent with the idea of a self-priming phosphorylation by PLK1 on T207.

To provide further evidence that the PLK1-mediated phosphorylation of BRCA2 favors BRCA2 binding, we performed an *in vitro* kinase assay followed by an amylose pull-down with recombinant proteins, and eluted the proteins with maltose. PLK1 was found in the maltose elution with WT-BRCA2$_{1-250}$ demonstrating that PLK1-phosphorylated BRCA2$_{1-250}$ binds to PLK1 (Figure 3C lane 4, Figure 3D). In contrast, the fraction of PLK1 in the eluate of T207A-BRCA2$_{1-250}$ was substantially reduced (Figure 3C, lane 6 compared to lane 4, Figure 3D) indicating that the phosphorylation of T207 is required for the efficient binding to PLK1 and confirming our previous results (Figure 3A, B).

**T207 is a *bona fide* docking site for PLK1**

To directly demonstrate the recognition of pT207 by PLK1, we measured the affinity of recombinant $PLK1_{PBD}$ for a synthetic 17 aa peptide comprising phosphorylated T207. Using isothermal titration calorimetry (ITC), we found that recombinant $PLK1_{PBD}$ bound to the T207 phosphorylated peptide with an affinity of $K_d$= 0.09 ± 0.01 µM (Figure 3E), similar to the optimal affinity reported for an interaction between $PLK1_{PBD}$ and its phosphorylated target(Elia et al., 2003b). Consistently, $PLK1_{PBD}$ bound to the fragment $BRCA2_{190-283}$ with nanomolar affinity upon phosphorylation by PLK1 ($K_d$= 0.14 ± 0.02 µM; Figure S3A) whereas it did not bind to the corresponding non-phosphorylated polypeptides (Figure 3F, Figure S3B). Mutation T207A also abolished the interaction (Figure 3G), in agreement with the pull-down experiments (Figure 3A-D). A peptide comprising pT207 and S206C mutation could not bind to $PLK1_{PBD}$ (Figure 3H), as predicted from the consensus sequence requirement for $PLK1_{PBD}$ interaction(Elia et al., 2003b). Last, a peptide containing phosphorylated S197, which is also a predicted docking site for PLK1, bound with much less affinity to $PLK1_{PBD}$ than pT207 ($K_d$= 17 ± 2 µM; Figure S3C).

To further characterize this molecular interaction, we determined the crystal structure of $PLK1_{PBD}$ bound to the T207 phosphorylated peptide at 3.1Å resolution (Table S2). Analysis of this 3D structure showed that, as expected, the 17 aa BRCA2 phosphopeptide binds in the cleft formed between the two Polo boxes (Figure 3I). Twelve residues of the peptide (from A199 to I210) are well-structured upon binding, burying about 694 $Å^2$ in the interface with $PLK1_{PBD}$. All BRCA2 residues from P202 to L209 are at least 25% buried in the complex. The interface is stabilized by 12 hydrogen bonds: the backbone of residues T200 to L209 as well as the side chain of

S206 are bonded to residues from Polo Box 1, whereas the side chain of phosphorylated T207 is bonded to residues from Polo Box 2 (see the zoom view in Figure 3I). Specifically, the backbone oxygen of T200 is bonded to the side chain of Y417 of $PLK1_{PBD}$. Residues L204, S205 and S206 form a β-sheet with residues W414, V415 and D416, characterized by hydrogen bonds between the backbone atoms of BRCA2 L204, S206 and PLK1 D416, W414, respectively. The side chain of S206 participates in 2 hydrogen-bonding interactions with the backbone of W414, which explains the strict requirement for this amino acid at this position(Elia et al., 2003b). Moreover, the phosphate group of pT207 participates in 3 hydrogen-bonding interactions with the side chains of residues H538, K540 and R557 in Polo Box 2 (see the zoom view in Figure 3I). This explains the critical dependence on phosphorylation for binding observed by ITC (Figure 3F-H). The presence of a buried leucine at the pT-3 position(Yun et al., 2009), as well as the electrostatic interactions of the serine at the pT-1 position with PLK1 W414(Elia et al., 2003b) and the phosphorylated threonine with PLK1 H538 and K540, have been described as essential for the high affinity and specificity of the interaction in other $PLK1_{PBD}$-phosphopeptide complexes (Elia et al., 2003b; García-Alvarez et al., 2007).

Thus, our biochemical and structural analysis demonstrate that the BRCA2 T207 phosphopeptide interacts with $PLK1_{PBD}$ as an optimal and specific $PLK1_{PBD}$ ligand. It supports a mechanism in which phosphorylation of T207 by PLK1 promotes the interaction of PLK1 with BRCA2 through a *bona fide* docking site for PLK1 and favours a cascade of phosphorylation events. In variants T200K and T207A the decrease in T207 phosphorylation impairs PLK1 docking at T207 explaining the reduction of binding to PLK1 and the global loss of phosphorylation by PLK1. S206C

eliminates the serine residue at -1 position required for $PLK1_{PBD}$ interaction resulting as well in a reduction of BRCA2 binding.

**Impairing T207 phosphorylation prolongs mitosis**

PLK1 is a master regulator of mitosis(Barr et al., 2004). To find out whether the interaction between BRCA2 and PLK1 is involved in the control of mitotic progression we examined the functional impact of two of the variants that reduce PLK1 phosphorylation at T207 (S206C and T207A) in the context of the full-length BRCA2 protein in cells. For this purpose, we generated stable cell lines expressing the BRCA2 cDNA coding for either the GFPMBP-BRCA2 WT or the variants to complement DLD1 BRCA2 deficient human cells (hereafter $BRCA2^{-/-}$). In this cell line, both alleles of BRCA2 contain a deletion in exon 11 causing a premature stop codon after BRC5 and cytoplasmic localization of a truncated form of the protein(Hucl et al., 2008). We selected two stable clones of each variant that show similar protein levels as the BRCA2 WT complemented cells (clone C1, hereafter BRCA2 WT) by western blot (Figure S4). We then tested the interaction of full-length BRCA2 with PLK1 in these stable clones by GFP pull-down. As expected, PLK1 readily co-purified with full-length BRCA2 WT from mitotic cells. Importantly, in cells expressing the variants S206C and T207A the level of co-purified PLK1 was greatly reduced (Figure 4A, B) confirming the results obtained with the overexpressed $BRCA2_{1-250}$ fragments (Figure 3A) now in the context of cells stably expressing the full-length BRCA2 protein. Thus, BRCA2 interaction with endogenous PLK1 is impaired in cells bearing variants S206C and T207A.

To examine the impact of BRCA2 variants on mitosis, we monitored the time individual cells spent in mitosis, from mitotic entry (defined as nuclear envelope break

down) to complete daughter cell separation using live cell imaging. Cells expressing the endogenous BRCA2 (hereafter $BRCA2^{+/+}$) and the BRCA2 WT cells showed similar kinetics, the majority of the cells (80% for $BRCA2^{+/+}$ and 82% for BRCA2 WT) having completed mitosis within 60 min (Figure 4C, 4D). In contrast, cells expressing variants S206C and T207A augmented the time spent in mitosis as manifested by a significant decrease in the frequency of cells dividing within 60 min (~49-51%), slightly higher than the $BRCA2^{-/-}$ cells (38%) (Figures 4C and 4D). The % of cell death during mitosis also increased in the mutated population compared to the BRCA2 WT complemented cells although the difference was not significant (Figure 4C, D). Representative videos of the still images shown in Figure 4C are included in Suppl. info. (movies S1-S4).

To find out the stage of mitosis at which the mutated cells were arrested we monitored the time elapsed from chromosome condensation to anaphase onset in cells labelled with SiR-DNA that allows visualizing the DNA in living cells. Interestingly, cells expressing S206C and T207A variants required significantly more time to reach anaphase (between 131 and 139 min) compared to the BRCA2 WT complemented cells (80 min) or $BRCA2^{+/+}$ cells (77 min) (Figure 4E, F). The $BRCA2^{-/-}$ also required more time on average (175 min) although the distribution of time in this population was variable, probably due to the different functions affected in BRCA2 deficient cells. Representative videos of the still images shown in Figure 4E are included in Suppl. info. (Movies S5-S7).

Taken together, cells expressing variants S206C and T207A display slower mitotic progression, specifically, from chromosome condensation to anaphase onset, compared to BRCA2 WT expressing cells.

**Docking of PLK1 at T207 of BRCA2 is required for the phosphorylation of BUBR1 at S676 and T680 by PLK1 and chromosome alignment**

BRCA2 interacts directly with BUBR1(Choi et al., 2012; Futamura et al., 2000). BUBR1 associates with and is phosphorylated by PLK1, which controls the stability of kinetochore-microtubule interactions and enables the alignment of chromosomes at the metaphase plate(Elowe et al., 2007; Suijkerbuijk et al., 2012). The delay in mitotic progression observed in the clones expressing S206C and T207A (Figure 4C-F) led us to investigate BUBR1 levels in these cell lines. As previously described(Elowe et al., 2007; Huang et al., 2008), upon cell arrest in G2/M phase by Nocodazole treatment, BUBR1 displayed 2 bands, the non-modified BUBR1 and the up-shifted band corresponding to phosphorylated BUBR1 (Figure 5A). Interestingly, the up-shifted band of BUBR1 strongly decreased in the cells expressing variants S206C or T207A compared to the cells expressing BRCA2 WT (Figure 5A, lane 3-6 compared to lane 2) and the same trend was observed in BRCA2$^{-/-}$ cells (Figure 5A, lane 8 compared to lanes 7 and 10). To find out the species of BUBR1 altered in the stable cells expressing the variants, we probed the same membrane with an antibody specific for pT680, a known BUBR1 phosphosite target of PLK1(Suijkerbuijk et al., 2012). Interestingly, both clones of the cells expressing variants S206C and T207A displayed reduced pT680 levels of BUBR1 (Figure 5A). As previously described(Suijkerbuijk et al., 2012), the phosphorylation of T680 is mediated by PLK1 since PLK1 inhibitors strongly reduced this signal (Figure S5A) and phosphatase treatment resulted in a decrease of the intensity of the band (Figure S5B) confirming the specificity of the anti-pT680-BUBR1 antibody in our cells. Furthermore, we observed a reduction in the PLK1-dependent phosphorylation of S676, another known target of PLK1 in BUBR1(Elowe et al., 2007) (Figure 5B), indicating that

BUBR1 phosphorylation by PLK1 is impaired in cells expressing BRCA2 variants S206C and T207A, at least at these two sites.

BUBR1 facilitates kinetochore-microtubules attachment via its interaction with the phosphatase PP2A-B56α which requires the phosphorylation of BUBR1 at the KARD motif comprising S676 and T680 (Suijkerbuijk et al., 2012). So we next tested whether BRCA2 and PLK1 formed a tetrameric complex with pT680-BUBR1 and PP2A-B56α. Interestingly, using a GFP pull-down to capture GFP-MBP-BRCA2 from mitotic cells the immunoprecipitated BRCA2 of BRCA2 WT complemented cells pulled-down PLK1, pT680-BUBR1 and PP2A-B56α (detected with an antibody against the catalytic subunit of PP2A, PP2AC), confirming the formation of a tetrameric complex. Importantly, cells expressing the variants S206C or T207A showed a strong reduction in the interaction of BRCA2 with PLK1 and pT680-BUBR1 in the context of the tetrameric complex and a strong reduction of PP2A-B56α interaction (Figure 5C, 5D). This is not due to a reduced localization of PLK1 or PP2A-B56α to the kinetochores in these cells, as the levels of these proteins at the kinetochores remain unchanged (Figure S6A-D).

The phosphorylation of BUBR1 at S676 and T680 by PLK1 and its association with PP2A-B56α are required for the formation of stable kinetochore-microtubules attachments(Elowe et al., 2007; Suijkerbuijk et al., 2012), a defect in this interaction results in chromosome misalignment. Therefore, we next examined whether cells expressing the BRCA2 variants S206C and T207A altered chromosome alignment. Following thymidine synchronization, the cells were blocked in prometaphase with Monastrol (Eg5 inhibitor) and then treated with proteasome inhibitor MG132 for 1h to avoid exit from mitosis. Chromosome alignment was subsequently analysed by

immunofluorescence. Strikingly, analysis of cells expressing S206C and T207A variants showed high frequency of faulty chromosome congression compared to the BRCA2 WT clone (52% in S206C A9, 42% in T207 B1 versus 16% in the BRCA2 WT clone) (Figure 5E, F) as detected by a signal of the centromere marker (CREST) outside the metaphase plate (Figure 5F). Interestingly, most of the misaligned chromosomes were located close to the spindle pole as revealed by the colocalization of CREST with the microtubule marker $\alpha$-tubulin (Figure 5E, 5F). Similar results were obtained when the cells were released from Monastrol treatment before adding the proteasome inhibitor MG132 to ensure they assemble a bipolar spindle (Figure S7A).

Together, our results show that the level of phosphorylation of BUBR1 by PLK1 is reduced in cells expressing the variants S206C and T207A suggesting that PLK1 needs to be bound to BRCA2 to efficiently phosphorylate BUBR1. Moreover, BRCA2 forms a tetrameric complex with pT680-BUBR1, PLK1 and PP2A-B56$\alpha$, a complex that is strongly impaired in the cells expressing variants S206C and T207A. As a consequence, these cells display severe chromosome misalignments.

**The BRCA2 variants that reduce PLK1 phosphorylation display a weaken SAC activity upon nocodazole induction, strong defects in chromosome segregation and aneuploidy**

In addition to allowing stable kinetochore-microtubules attachments, BUBR1 is an essential component of the spindle assembly checkpoint (SAC) (Sudakin et al., 2001). Although closely related, these activities of BUBR1 can be uncoupled and both are required for faithful chromosome segregation (Zhang et al., 2016). In view of the interaction of BRCA2 with BUBR1(Choi et al., 2012; Futamura et al., 2000) and

the impact of BRCA2 on BUBR1 phosphorylation (Figure 5A-C), we next assessed the SAC activity of these cells by measuring the percentage of cells arrested in mitosis after treatment with the spindle poison nocodazole (Figure 7A). A previous work has used the percentage of cells expressing the mitotic marker histone 3 phosphorylated at S10 (pH3, S10) (Giet and Glover, 2001) by flow cytometry as a marker of SAC activity in BRCA2 deficient cells (Choi et al., 2012). We used the same method to monitor the SAC activity of our mutated cells. As expected, the percentage of pH3 positive BRCA2 WT cells upon nocodazole treatment increased compared to non-treated cells, this increase was similar to the one observed in cells expressing endogenous BRCA2 ($BRCA2^{+/+}$) whereas in BRCA2 deficient cells ($BRCA2^{-/-}$) the percentage was significantly lower as previously described (Figure 6A, Figure S7B, C) (Choi et al., 2012). Interestingly, the stable cell lines expressing variants S206C and T207A showed a significant decrease in the percentage of mitotic cells after nocodazole treatment in comparison to the BRCA2 WT cells, indicating a weaken SAC activity under induced mitotic-arrest conditions (Figure 6A). Consistently, a smaller percentage of G2/M cells was observed in cells bearing BRCA2 S206C and T207A variants compared to the BRCA2 WT counterpart upon mitotic arrest induction (Figure S7D). The reduced number of cells in G2/M was not due to a defective cell cycle profile as the distribution of these cells in unchallenged conditions was equivalent to that of the WT cells (Figure S7E).

Thus, in response to microtubule poison, VUS S206C and T207A compromise SAC activity, which results in a weaken ability to induce mitotic arrest.

Unresolved chromosome misalignment as observed in these cells together with a weaken SAC activity is expected to drive chromosome missegregation. To find out if

this was the case in cells expressing BRCA2 variants S206C and T207A we next examined chromosome segregation by immunofluorescence in cells synchronized by double-thymidine block and released for 15h to enrich the cell population at anaphase/telophase stage. In cells expressing S206C and T207A, 49% and 36%, respectively, displayed chromosome segregation errors compared to 20% of the cells expressing BRCA2 WT, these included lagging chromosomes and chromosome bridges (Figure 6B, C).

Erroneous chromosome segregation generates aneuploid cells during cell division(Santaguida and Amon, 2015). Given the strong chromosome segregation defects observed in cells expressing S206C and T207A we next analysed the number of chromosomes in these cells. Total chromosome counts carried out on metaphase spreads revealed that 37.1% of BRCA2 WT cells exhibited aneuploidy with chromosome losses or gains. In the case of S206C A7 and T207A B1, this number was elevated to 52.2% and 61.8% of the cells, respectively (Figure 7A). An example of the images analyzed can be found in Figure 7B. As the number of chromosomes was difficult to assess for cells with high content of chromosome gains we arbitrarily discarded cells that contained more than 65 chromosomes. Thus, tetraploid cells were not included in this measurement. Therefore, as a complementary test, we determined the frequency of tetraploid cells by assessing the incorporation of BrdU of asynchronous cell populations and measuring the frequency of S-phase cells with >4N DNA content (Figure 7C). The quantification of this data shows that similar to the BRCA2 WT complemented cells, the frequency of tetraploidy in cells bearing the variants is <1% of the total population (Figure 7D) while the frequency of BrdU positive cells was equivalent between the BRCA2 WT and the VUS expressing cells (Figure S8A-D).

Together, these results indicate that, in addition to the severe chromosome misalignment phenotype, cells expressing S206C and T207A display high frequency of chromosome missegregation in double thymidine-synchronized cells and a weaken SAC activity in nocodazole-induced mitotic arrested cells. As a consequence, the incidence of aneuploidy, but not tetraploidy, is greatly exacerbated in these cells.

**The BRCA2 variants altering PLK1 phosphorylation restore the hypersensitivity of BRCA2 deficient cells to DNA damage and PARP inhibition**

Since BRCA2 has a major role in DNA repair by HR, the prolonged mitosis observed in the VUS-expressing cell lines (Figure 4) could result from checkpoint activation through unrepaired DNA. In addition, defects in chromosome segregation have been reported as a cause of DNA damage(Janssen et al., 2011). To test the DNA repair efficiency of the cell lines expressing variants S206C and T207A, we performed a clonogenic survival assay in the stable clones after treatment with mitomycin C (MMC), an inter-strand crosslinking agent to which BRCA2 deficient cells are highly sensitive(Kraakman-van der Zwet et al., 2002). As expected, BRCA2 deficient cells ($BRCA2^{-/-}$) showed hypersensitivity to MMC treatment whereas BRCA2 WT cells complemented this phenotype almost to the same survival levels as the cells expressing the endogenous BRCA2 ($BRCA2^{+/+}$). The stable clones expressing variants S206C and T207A also complemented the hypersensitive phenotype of BRCA2 deficient cells ($BRCA2^{-/-}$) reaching similar levels as the BRCA2 WT clone (BRCA2 WT) (Figure 8A) suggesting that the delay in mitosis is not a consequence of checkpoint activation via unrepaired DNA. In contrast, clones expressing VUS S206C and T207A did show a growth defect manifested in a reduced number of

colonies observed in unchallenged cells (Figure S9A), which is consistent with the mitotic phenotype observed (Figure 4-6). To exclude a possible bias arising from the different ability to form colonies of these cells we also tested the sensitivity to MMC of the cell population by MTT assay. As shown in Figure 8B, cells expressing S206C and T207A showed similar relative viability compared to BRCA2 WT complemented cells or the cells expressing endogenous BRCA2 ($BRCA2^{+/+}$), confirming our results. To additionally address the DNA repair capacity of these cells, we tested their viability in upon treatment with the poly (ADP-ribose) polymerase (PARP) inhibitor Olaparib. PARP1 is an enzyme required for the sensing of DNA single strand breaks (SSBs) and double strand breaks (DSBs) that becomes essential in the absence of a functional HR pathway (Bryant et al., 2005) and therefore is used as a surrogate of HR proficiency. In fact, PARP1 inhibitors, in particular Olaparib, are currently used in the clinic to treat breast and ovarian cancer patients carrying germline mutations in BRCA1/2. In our settings, the relative viability of $BRCA2^{-/-}$ cells was 45% upon 4-day treatment with the highest Olaparib concentration tested (5 µM); in contrast, 74% of BRCA2 WT complemented cells remained viable. Similarly, cells expressing S206C or T207A survived the treatment equally well as the cells expressing BRCA2 WT, the percentage of viable cells at 5 µM treatment ranging from 70 to 83 % depending on the clone (Figure 8C) indicating that the mutated cells can rescue the phenotype of $BRCA2^{-/-}$ cells.

Finally, to determine directly the levels of spontaneous DNA damage in these cells and whether or not they can recruit RAD51 to sites of DNA damage we measured both the number of cells containing more than 10 nuclear foci of the DSB marker γH2AX and the ratio of RAD51/γH2AX foci per nucleus, in cells unchallenged or 2h upon induction of DNA damage by ionizing radiation (6 Gy), (+IR). Our results show

that the number of γH2AX foci, indicative of spontaneous DNA damage, is not increased in cells expressing S206C compared to the BRCA2 WT complemented cells and is increased to similar levels in cells expressing BRCA2 WT or S206C upon irradiation (Figure 8D). We noticed that the number of nuclear γH2AX foci in BRCA2$^{-/-}$ was remarkably similar to that of the BRCA2 WT cells; this is probably due to the adaptation of these cells to BRCA2 deficiency as opposed to a transient depletion.

Importantly, cells expressing S206C showed equivalent ratio of RAD51/γH2AX foci per nucleus following irradiation than in the BRCA2 WT cells indicating that, in these cells, BRCA2 can recruit RAD51 to the DNA damage sites. This is in contrast to the BRCA2$^{-/-}$ cells where the ratio of RAD51/γH2AX foci per nucleus in irradiated conditions is nearly zero (Figure 8E and Figure S9B).

In summary, these results indicate that the role of BRCA2 in conjunction with PLK1 in mitosis is independent of the HR function of BRCA2 as the variants S206C and T207A affecting PLK1 phosphorylation of BRCA2 are not sensitive to DNA damage and are able to recruit RAD51 to DNA damage sites (as shown for S206C).

## Discussion

Our results demonstrate that residues S193 and T207 of BRCA2 can be phosphorylated by PLK1 (Figure 2) and that pT207 constitutes a *bona fide* docking site for PLK1$_{PBD}$ (Figure 3F-I). Accordingly, *BRCA2* missense variants of unknown clinical significance reducing the phosphorylation status of T207 (T207A, S206C, T200K), result in a decrease in the interaction of BRCA2-PLK1 (Figure 3A-I, 4A). The phenotype of cells expressing two of these breast cancer variants (S206C, T207A) in a BRCA2 deficient background, allowed us to investigate in detail the possible role of BRCA2 phosphorylation by PLK1 in the control of mitosis. Unexpectedly, we found

that the cells expressing S206C and T207A display defective chromosome congression to the metaphase plate (Figure 5E, F) causing a delay in mitosis progression (Figure 4C, D), particularly from chromosome condensation to anaphase onset (Figure 4E, F). Remarkably, variants S206C and T207A of BRCA2 led to a frequency of chromosome misalignment equivalent to the one reported for BUBR1 mutated in the three phosphorylation targets sites of PLK1, BUBR1 3A mutant(Suijkerbuijk et al., 2012).

Mechanistically, cells expressing T207A and S206C exhibit reduced PLK1-dependent BUBR1 phosphorylation at two known tension-sensitive phosphosites required for the establishment of kinetochore-microtubule attachments, S676 and T680(Elowe et al., 2007; Suijkerbuijk et al., 2012) (Figure 5A, B). Proper kinetochore-microtubule attachments also require the interaction of BUBR1 with the phosphatase PP2A-B56$\alpha$ to balance Aurora B kinase activity(Foley et al., 2011; Suijkerbuijk et al., 2012). This interaction is mediated through the phosphorylation of KARD motif of BUBR1 by PLK1. Accordingly, we found that BRCA2 forms a tetrameric complex with PLK1-pBUBR1-PP2A-B56$\alpha$ and that BRCA2 variants S206C and T207A exhibit a strongly reduce the interaction with PLK1, pBUBR1 and PP2A-B56$\alpha$ in this complex (Figure 5C, D). The fact that the signal of PP2A-B56$\alpha$ at the kinetochores is unchanged in the mutated cells (Figure S6) suggests that is the impaired interaction of PP2A-B56$\alpha$ with pBUBR1 (in complex with BRCA2 and PLK1) rather than the recruitment of PP2A-B56$\alpha$ to the kinetochores *per se* is what is responsible for the phenotype observed in these cells.

The increased mitotic delay resulting from chromosome alignment defects is indicative of a functional SAC. However, upon induced mitotic arrest by nocodazole,

these cells display weaken SAC activity as manifested in a reduced frequency of mitotic cells (Figure 6A), denoting that the mitotic checkpoint is not fully activated under these conditions. These two opposing phenotypes are intriguing; however, the fact that there are two pools of BUBR1 with different functions; one important for the stability of kinetochore-microtubule interactions and another involved in SAC activation[16,17] leads us to speculate that the reduced phosphorylation of BUBR1 may unbalance the pool of BUBR1 that is required for full activation of SAC. Moreover, based on the strong delay in mitosis we observe, we believe the effect in SAC activity is probably a consequence of the misalignment phenotype.

As a consequence of the chromosome misalignment and the weaken SAC activity, cells bearing T207A and S206C variants display chromosome segregation errors including lagging chromosomes and chromosome bridges (Figure 6B, C). Importantly, these accumulated errors ultimately lead to a broad spectrum of chromosome gains and losses (aneuploidy) compared to the wild type counterpart (Figure 7A), but not to tetraploid cells (Figure 7C), suggesting that cytokinesis *per se*, is not affected.

Finally, the function of BRCA2-PLK1 interaction in mitosis is independent of the HR function of BRCA2 as cells expressing these variants display normal sensitivity to DNA damage (MMC) and PARP inhibitors (Figure 8A-C) and the recruitment of RAD51 to DNA damage sites remains intact (Figure 8E, Figure S9B).

Putting our results together we propose the following model (Figure 8F): In cells expressing BRCA2 WT, PLK1 phosphorylates BRCA2 on T207 leading to the docking of PLK1 at this site. This step promotes the phosphorylation of BUBR1 at the tension-sensitive phosphosites (S676 and T680) by PLK1 in prometaphase allowing

the interaction of BUBR1 with the phosphatase PP2A-B56α to balance Aurora B activity (Figure 8F, panel 1). Once the kinetochore-microtubules attachments are established and proper tension is achieved, BUBR1 is no longer phosphorylated by PLK1(Elowe et al., 2007). This leads to a full alignment of chromosomes at the metaphase plate (Figure 8F, panel 2) and the subsequent faithful chromosome segregation in anaphase (Figure 8F, panel 3).

In cells expressing the variants that impair T207 phosphorylation (T200K, S206C, T207A), PLK1 cannot be recruited to pT207-BRCA2, impairing the phosphorylation of BUBR1 by the same kinase (Figure 8F, panel 1'), reducing PP2A-B56α interaction, thus leading to chromosome misalignment defects that prolong mitosis (Figure 8F, panel 2'); as a consequence, these cells exhibit increased chromosome segregation errors (Figure 8F, panel 3') and aneuploidy.

Our results are consistent with the "processive phosphorylation" model (as opposed to the "distributive phosphorylation" model) proposed before on how $PLK1_{PBD}$ regulates the kinase activity of PLK1(Lowery et al., 2005), with some modifications. In this model, $PLK1_{PBD}$ would first bind the site phosphorylated by another mitotic kinase allowing the kinase domain of PLK1 to phosphorylate the same protein at another site. In this work, we show that the mitotic kinase would be PLK1 itself ("self-priming"(Kang et al., 2006)), and the kinase domain of PLK1 would phosphorylate not the same protein but BUBR1 bound to BRCA2. Interestingly, the consensus sequence of PLK1 phosphorylation imposes an aspartic or glutamic acid at the -2 position instead of a serine (S205)(Nakajima et al., 2003). Thus, this work extends the consensus sequence of PLK1 phosphorylation.

In all, we reveal an unexpected chromosome stability control mechanism that

depends on the phosphorylation of BRCA2 by PLK1 at T207. We show that BRCA2 pT207 is a docking platform for PLK1 that ensures the efficient phosphorylation of BUBR1 required for PP2A-B56α phosphatase interaction through the formation of a tetrameric complex comprising BRCA2-PLK1-pBUBR1-PP2A-B56α. Why is BRCA2 required for PP2A-B56α interaction with pBUBR1? One possibility is that BRCA2 directly binds PP2A-B56α. In support of this hypothesis, a previous report has shown that BRCA2 contains a putative binding motif specific for PP2A-B56α (Hertz et al., 2016). Either by direct binding to PP2A-B56α or by favoring pBUBR1-PP2A-B56α interaction within the tetrameric complex, BRCA2 ensures a proper balance of kinases and phosphatases at the kinetochore required for the faithful segregation of DNA content to daughter cells; a function that is separate from its HR activity.

BRCA2 harbours another docking site for PLK1 at T77, a site that is primed by CDK phosphorylation (Yata et al., 2014). In this study we observed, in addition to T207, several phosphorylation events including S193 (Figure 2) which is required for the midbody localization of BRCA2 (Takaoka et al., 2014). Furthermore, other PLK1-phosphorylation sites have been described in the central region of BRCA2 (Lee et al., 2004). However, the chronology of phosphorylation events and how the activities they regulate are coordinated throughout the cell cycle deserve further study. The recent findings of a mitotic-specific and DNA-repair independent function of the DNA checkpoint kinase ATR (Kabeche et al., 2018) together with previous and recent work implicating PLK1 in DNA repair checkpoint recovery (Smits et al., 2000) and promoting alternative end-joining via phosphorylation of CtIP in mitosis (Wang et al., 2018) suggest that the processes of DNA repair and cell division may involve common players acting on different protein networks exquisitely regulated via post-translational modifications.

We showed here that *BRCA2* missense variants identified in breast cancer patients affect BRCA2 phosphorylation by PLK1 with direct consequences on chromosome stability manifested by chromosome missegregation and aneuploidy. Although these individual variants are rare (Table S1), the majority of pathogenic mutations recorded to date lead to a truncated protein either not expressed or mislocalized (Spain et al., 1999) which would be predicted to affect this function. Consistent with this idea, the BRCA2$^{-/-}$ deficient cells used in this study exhibit low levels of phosphorylated BUBR1 (Figure 5A lane 8 vs lane 10). Thus, the chromosome alignment function described here could be responsible for the numerical chromosomal aberrations observed in *BRCA2*-associated tumors(Gretarsdottir et al., 1998).

Finally, the lack of sensitivity to the PARP inhibitor Olaparib have important clinical implications as breast cancer patients carrying these variants are not predicted to respond to this type of treatment (unlike *BRCA2*-mutated tumors that are HR-deficient).

**Author Contributions**

A.E. purified WT and mutated BRCA2$_{1\text{-}250}$, established the stable DLD1$^{-/-}$ cell lines, performed kinase assays, pull-down assays, western blots, time-lapse microscopy experiments, mitotic index measurements by FACS, clonogenic survival and MTT assays as well as the statistical analysis for these experiments. C.M. performed IF and image acquisition of metaphase plate alignment, chromosome segregation and karyotype analysis. M.J. performed the NMR experiments assisted by S. M., F.T. and S.Z.J. S.M. purified PLK1$_{PBD,}$ performed the ITC experiments and solved the X-ray structure assisted by V.R. V.B. assisted establishing stable clones and performing

clonogenic survival assays. P.D. purified $PLK1_{PBD}$. A.M. cloned and produced PLK1 and PLK1-KD from insect cells. A.C., A.E. and S.Z.J. designed the experiments. A.C. and S.Z.J. supervised the work. A.C. wrote the paper with important contributions from all authors.

**Acknowledgments**

We thank members of the AC lab for fruitful comments on the manuscript and Davide Panigada for the illustration of chromosomes in Figure 8. We thank Rene H. Medema for useful discussions on this work including the cell synchronization protocol used in Figure 7. We also thank Juan S. Martinez for construct $BRCA2_{1-250}$, Anne Houdusse for construct $PLK1_{365-603}$, Eric Nigg for pS676-BUBR1 antibody. We acknowledge the Cell and Tissue Imaging Facility of the Institut Curie (PICT), a member of the France BioImaging National Infrastructure (ANR-10-INBS-04) and the French Infrastructure for Integrated Structural Biology (https://www.structuralbiology.eu/networks/frisbi, (ANR-10-INSB-05-01). We thank Charlene Lasgi from the Flow Cytometry platform of Institut Curie, Orsay.

This work was supported by the ATIP-AVENIR CNRS/INSERM Young Investigator grant 201201, EC-Marie Curie Career Integration grant CIG293444 to A.C. and Institut National du Cancer INCa-DGOS_8706 to A.C. and S.Z.J.; A.E. was supported by the Swedish Society for Medical Research.

The authors declare no conflict of interest.

Correspondence and requests for materials should be addressed to A.C.

**References**

Barr, F.A., Silljé, H.H.W., Nigg, E.A., 2004. Polo-like kinases and the orchestration of cell division. Nat Rev Mol Cell Biol 5, 429–440.

Béroud, C., Letovsky, S.I., Braastad, C.D., Caputo, S.M., Beaudoux, O., Bignon, Y.-J., Bressac-de-Paillerets, B., Bronner, M., Buell, C.M., Collod-Béroud, G., Coulet, F., Derive, N., Divincenzo, C., Elzinga, C.D., Garrec, C., Houdayer, C., Karbassi, I., Lizard, S., Love, A., Muller, D., Nagan, N., Nery, C.R., Rai, G., Révillion, F., Salgado, D., Sevenet, N., Sinilnikova, O., Sobol, H., Stoppa-Lyonnet, D., Toulas, C., Trautman, E., Vaur, D., Vilquin, P., Weymouth, K.S., Willis, A., Laboratory Corporation of America Variant Classification Group, Quest Diagnostics Variant Classification Group, UNICANCER Genetic Group BRCA Laboratory Network, Eisenberg, M., Strom, C.M., 2016. BRCA Share: A Collection of Clinical BRCA Gene Variants. Hum. Mutat. 37, 1318–1328.

Bryant, H.E., Schultz, N., Thomas, H.D., Parker, K.M., Flower, D., Lopez, E., Kyle, S., Meuth, M., Curtin, N.J., Helleday, T., 2005. Specific killing of BRCA2-deficient tumours with inhibitors of poly(ADP-ribose) polymerase. Nature 434, 913–917.

Choi, E., Park, P.-G., Lee, H.-O., Lee, Y.-K., Kang, G.H., Lee, J.W., Han, W., Lee, H.C., Noh, D.-Y., Lekomtsev, S., Lee, H., 2012. BRCA2 fine-tunes the spindle assembly checkpoint through reinforcement of BubR1 acetylation. Developmental Cell 22, 295–308.

Daniels, M.J., Wang, Y., Lee, M., Venkitaraman, A.R., 2004. Abnormal cytokinesis in cells deficient in the breast cancer susceptibility protein BRCA2. Science 306, 876–879.

Elia, A.E.H., Cantley, L.C., Yaffe, M.B., 2003a. Proteomic screen finds pSer/pThr-binding domain localizing Plk1 to mitotic substrates. Science 299, 1228–1231.

Elia, A.E.H., Rellos, P., Haire, L.F., Chao, J.W., Ivins, F.J., Hoepker, K., Mohammad, D., Cantley, L.C., Smerdon, S.J., Yaffe, M.B., 2003b. The molecular basis for phosphodependent substrate targeting and regulation of Plks by the Polo-box domain. Cell 115, 83–95.

Elowe, S., Dulla, K., Uldschmid, A., Li, X., Dou, Z., Nigg, E.A., 2010. Uncoupling of the spindle-checkpoint and chromosome-congression functions of BubR1. J Cell Sci 123, 84–94.

Elowe, S., Hümmer, S., Uldschmid, A., Li, X., Nigg, E.A., 2007. Tension-sensitive Plk1 phosphorylation on BubR1 regulates the stability of kinetochore microtubule interactions. Genes Dev 21, 2205–2219.

Foley, E.A., Maldonado, M., Kapoor, T.M., 2011. Formation of stable attachments between kinetochores and microtubules depends on the B56-PP2A phosphatase. Nat Cell Biol 13, 1265–1271.

Futamura, M., Arakawa, H., Matsuda, K., Katagiri, T., Saji, S., Miki, Y., Nakamura, Y., 2000. Potential role of BRCA2 in a mitotic checkpoint after phosphorylation by hBUBR1. Cancer Res 60, 1531–1535.

García-Alvarez, B., de Cárcer, G., Ibañez, S., Bragado-Nilsson, E., Montoya, G., 2007. Molecular and structural basis of polo-like kinase 1 substrate recognition: Implications in centrosomal localization. Proc Natl Acad Sci USA 104, 3107–3112.

Giet, R., Glover, D.M., 2001. Drosophila Aurora B Kinase Is Required for Histone H3 Phosphorylation and Condensin Recruitment during Chromosome Condensation and to Organize the Central Spindle during Cytokinesis. J Cell Biol 152, 669–682.

Golsteyn, R.M., Mundt, K.E., Fry, A.M., Nigg, E.A., 1995. Cell cycle regulation of the activity and subcellular localization of Plk1, a human protein kinase implicated in mitotic spindle function. J Cell Biol 129, 1617–1628.

Gretarsdottir, S., Thorlacius, S., Valgardsdottir, R., Gudlaugsdottir, S., Sigurdsson, S., Steinarsdottir, M., Jonasson, J.G., Anamthawat-Jonsson, K., Eyfjord, J.E., 1998. BRCA2 and p53 Mutations in Primary Breast Cancer in Relation to Genetic Instability. Cancer Res 58, 859–862.

Hauf, S., Cole, R.W., LaTerra, S., Zimmer, C., Schnapp, G., Walter, R., Heckel, A., van Meel, J., Rieder, C.L., Peters, J.-M., 2003. The small molecule Hesperadin reveals a role for Aurora B in correcting kinetochore-microtubule attachment and in maintaining the spindle assembly checkpoint. J Cell Biol 161, 281–294.

Hertz, E.P.T., Kruse, T., Davey, N.E., López-Méndez, B., Sigurðsson, J.O., Montoya, G., Olsen, J.V., Nilsson, J., 2016. A Conserved Motif Provides Binding Specificity to the PP2A-B56 Phosphatase. Mol. Cell 63, 686–695.

Huang, H., Hittle, J., Zappacosta, F., Annan, R.S., Hershko, A., Yen, T.J., 2008. Phosphorylation sites in BubR1 that regulate kinetochore attachment, tension, and mitotic exit. The Journal of Cell Biology 183, 667–680.

Hucl, T., Rago, C., Gallmeier, E., Brody, J.R., Gorospe, M., Kern, S.E., 2008. A syngeneic variance library for functional annotation of human variation: application to BRCA2. Cancer Res 68, 5023–5030.

Janssen, A., van der Burg, M., Szuhai, K., Kops, G.J.P.L., Medema, R.H., 2011. Chromosome Segregation Errors as a Cause of DNA Damage and Structural Chromosome Aberrations. Science 333, 1895–1898.

Jensen, R.B., Carreira, A., Kowalczykowski, S.C., 2010. Purified human BRCA2 stimulates RAD51-mediated recombination. Nature 467, 678–683.

Kabeche, L., Nguyen, H.D., Buisson, R., Zou, L., 2018. A mitosis-specific and R loop-driven ATR pathway promotes faithful chromosome segregation. Science 359, 108–114.

Kang, Y.H., Park, J.-E., Yu, L.-R., Soung, N.-K., Yun, S.-M., Bang, J.K., Seong, Y.-S., Yu, H., Garfield, S., Veenstra, T.D., Lee, K.S., 2006. Self-regulated Plk1 recruitment to kinetochores by the Plk1-PBIP1 interaction is critical for proper chromosome segregation. Mol. Cell 24, 409–422.

Kraakman-van der Zwet, M., Overkamp, W.J.I., van Lange, R.E.E., Essers, J., van Duijn-Goedhart, A., Wiggers, I., Swaminathan, S., van Buul, P.P.W., Errami, A., Tan, R.T.L., Jaspers, N.G.J., Sharan, S.K., Kanaar, R., Zdzienicka, M.Z., 2002. Brca2 (XRCC11) deficiency results in radioresistant DNA synthesis and a higher frequency of spontaneous deletions. Mol. Cell. Biol. 22, 669–679.

Lee, M., Daniels, M.J., Venkitaraman, A.R., 2004. Phosphorylation of BRCA2 by the Polo-like kinase Plk1 is regulated by DNA damage and mitotic progression. Oncogene 23, 865–872.

Lin, H.-R., Ting, N.S.Y., Qin, J., Lee, W.-H., 2003. M phase-specific phosphorylation of BRCA2 by Polo-like kinase 1 correlates with the dissociation of the BRCA2-P/CAF complex. J Biol Chem 278, 35979–35987. doi:10.1074/jbc.M210659200

Lowery, D.M., Lim, D., Yaffe, M.B., 2005. Structure and function of Polo-like kinases. Oncogene 24, 248–259.

Mondal, G., Rowley, M., Guidugli, L., Wu, J., Pankratz, V.S., Couch, F.J., 2012. BRCA2 localization to the midbody by filamin A regulates cep55 signaling and completion of cytokinesis. Developmental Cell 23, 137–152.

Moynahan, M.E., Pierce, A.J., Jasin, M., 2001. BRCA2 is required for homology-directed repair of chromosomal breaks. Molecular Cell 7, 263–272.

Nakajima, H., Toyoshima-Morimoto, F., Taniguchi, E., Nishida, E., 2003. Identification of a consensus motif for Plk (Polo-like kinase) phosphorylation reveals Myt1 as a Plk1 substrate. J Biol Chem 278, 25277–25280.

Neef, R., Preisinger, C., Sutcliffe, J., Kopajtich, R., Nigg, E.A., Mayer, T.U., Barr, F.A., 2003. Phosphorylation of mitotic kinesin-like protein 2 by polo-like kinase 1 is required for cytokinesis. J Cell Biol 162, 863–875.
Park, I., Kwon, M.-S., Paik, S., Kim, H., Lee, H.-O., Choi, E., Lee, H., 2017. HDAC2/3 binding and deacetylation of BubR1 initiates spindle assembly checkpoint silencing. FEBS J 284, 4035–4050.
Saleh-Gohari, N., Helleday, T., 2004. Conservative homologous recombination preferentially repairs DNA double-strand breaks in the S phase of the cell cycle in human cells. Nucleic Acids Research 32, 3683–3688. d
Santaguida, S., Amon, A., 2015. Short- and long-term effects of chromosome mis-segregation and aneuploidy. Nat Rev Mol Cell Biol 16, 473–485.
Smits, V.A., Klompmaker, R., Arnaud, L., Rijksen, G., Nigg, E.A., Medema, R.H., 2000. Polo-like kinase-1 is a target of the DNA damage checkpoint. Nat Cell Biol 2, 672–676.
Spain, B.H., Larson, C.J., Shihabuddin, L.S., Gage, F.H., Verma, I.M., 1999. Truncated BRCA2 is cytoplasmic: implications for cancer-linked mutations. Proc Natl Acad Sci USA 96, 13920–13925.
Sudakin, V., Chan, G.K., Yen, T.J., 2001. Checkpoint inhibition of the APC/C in HeLa cells is mediated by a complex of BUBR1, BUB3, CDC20, and MAD2. J Cell Biol 154, 925–936.
Suijkerbuijk, S.J.E., Vleugel, M., Teixeira, A., Kops, G.J.P.L., 2012. Integration of kinase and phosphatase activities by BUBR1 ensures formation of stable kinetochore-microtubule attachments. Developmental Cell 23, 745–755.
Szabo, C., Masiello, A., Ryan, J.F., Brody, L.C., 2000. The breast cancer information core: database design, structure, and scope. Hum. Mutat. 16, 123–131.
Takaoka, M., Saito, H., Takenaka, K., Miki, Y., Nakanishi, A., 2014. BRCA2 phosphorylated by PLK1 moves to the midbody to regulate cytokinesis mediated by nonmuscle myosin IIC. Cancer Res 74, 1518–1528.
Wang, H., Qiu, Z., Liu, B., Wu, Y., Ren, J., Liu, Y., Zhao, Y., Wang, Y., Hao, S., Li, Z., Peng, B., Xu, X., 2018. PLK1 targets CtIP to promote microhomology-mediated end joining. Nucleic Acids Research.
Yata, K., Bleuyard, J.-Y., Nakato, R., Ralf, C., Katou, Y., Schwab, R.A., Niedzwiedz, W., Shirahige, K., Esashi, F., 2014. BRCA2 coordinates the activities of cell-cycle kinases to promote genome stability. CellReports 7, 1547–1559.
Yun, S.-M., Moulaei, T., Lim, D., Bang, J.K., Park, J.-E., Shenoy, S.R., Liu, F., Kang, Y.H., Liao, C., Soung, N.-K., Lee, S., Yoon, D.-Y., Lim, Y., Lee, D.-H., Otaka, A., Appella, E., McMahon, J.B., Nicklaus, M.C., Burke, T.R., Yaffe, M.B., Wlodawer, A., Lee, K.S., 2009. Structural and functional analyses of minimal phosphopeptides targeting the polo-box domain of polo-like kinase 1. Nat Struct Mol Biol 16, 876–882.
Zhang, G., Mendez, B.L., Sedgwick, G.G., Nilsson, J., 2016. Two functionally distinct kinetochore pools of BubR1 ensure accurate chromosome segregation. Nature Communications 7, 12256.
Zitouni, S., Nabais, C., Jana, S.C., Guerrero, A., Bettencourt-Dias, M., 2014. Polo-like kinases: structural variations lead to multiple functions. Nat Rev Mol Cell Biol 15, 433–452.

## Figure legends

### Figure 1. BRCA2 VUS alter PLK1 phosphorylation of $BRCA2_{1-250}$

**(A)** PLK1 *in vitro* kinase assay with $BRCA2_{1-250}$. Top: The polypeptides encompassing 2x-MBP-$BRCA2_{1-250}$ WT or S193A, M192T, S196N, T200K, S206C, T207A mutations were incubated with recombinant PLK1 in the presence of $\gamma^{32}$P-ATP. The samples were resolved on 7.5% SDS-PAGE and the $^{32}$P-labeled products were detected by autoradiography. Bottom: 7.5% SDS-PAGE showing the input of purified 2xMBP-$BRCA2_{1-250}$ WT and mutated proteins (0.5 µg) used in the reaction as indicated. **(B)** Quantification of the relative phosphorylation in (A). Data in (b) are represented as mean ± SD from at least four independent experiments (WT (n=9), S193A (n=4), M192T (n=4), S196N (n=4), S206C (n=4), T200K (n=5), T207A (n=4)). **(C)** PLK1 *in vitro* kinase assay performed as in (a) with recombinant PLK1 or the PLK1 kinase dead K82R mutant (PLK1-KD) together with $BRCA2_{1-250}$ WT as substrate, in the presence or absence of the PLK1 inhibitor Bi2536 (50 nM) in the kinase reaction buffer. **(D)** Quantification of the relative phosphorylation in (C). Data in (D) are represented as mean ± SD from three independent experiments. (B and C) One-way ANOVA test with Tukey's multiple comparisons test was used to calculate statistical significance of differences (the p-values show differences compared to WT; ns (non-significant)).

### Figure 2. PLK1 phosphorylates T207 in $BRCA2_{190-283}$

Phosphorylation kinetics of $BRCA2_{190-283}$ as observed by NMR. **(A)** Superposition of the $^{1}$H-$^{15}$N HSQC spectra recorded as a function of the phosphorylation time: from black (before phosphorylation) to red (after 24h with PLK1). PLK1 (1.1 µM) was

incubated with $^{15}N$ labelled $BRCA2_{190-283}$ (200 µM) at pH 7.8 and 303 K. For each time point, 140 µl were taken, the sample was heated during 10 min at 368 K, 10% D2O were added and the pH was adjusted to 7.0. Right panel: Zoom on the region containing the NMR signals of the phosphorylated residues. NMR peaks are labelled to indicate the corresponding residue following the timing colour code indicated in the left arrow (dark blue label: peaks appearing before 4 h; green label: peaks appearing before 5 h; red label: peaks observed only at 24 h). pT219 and pT226 give rise to several peaks (marked as (A), (B), (C)) as a function of the phosphorylation state of the surrounding residues. **(B)** Phosphorylation kinetics of S193 (red), T207 (black), T219 (blue) and T226 (grey). In the case of T226, the phosphorylation percentage corresponds to the sum of the intensities of peaks pT226(a), pT226(b) and pT226(C), which reflects the existence of different environments for phosphorylated T226 due to further phosphorylation of neighbouring T219 and S231. The multiplicity of the peaks corresponding to phosphorylated T226 at 24h hindered a proper measurement of this time point. **(C)** Superposition of the $^{1}H$-$^{15}N$ HSQC spectra recorded on VUS T207A as a function of the phosphorylation time: from black (before phosphorylation) to red (after 24h incubation with PLK1). The conditions are the same as in Figure 2A. A zoom on the region containing the NMR signals of the phosphorylated residues is shown. **(D)** Phosphorylation kinetics of T207 (black), S193 (red), T226 (grey) and T219 (blue), in WT (filled circles) versus T207A mutated $BRCA2_{190-283}$ (empty circles). **(E)** Superposition of the $^{1}H$-$^{15}N$ HSQC spectra recorded on variant T200K as a function of the phosphorylation time. **(F)** Phosphorylation kinetics of T207 (black), S193 (red), T226 (grey) and T219 (blue), in WT (filled circles) versus T200K mutated $BRCA2_{190-283}$ (empty circles).

**Figure 3. BRCA2 variants showing reduced phosphorylation by PLK1 impair PLK1 binding**

**(A)** 2xMBP-BRCA2$_{1-250}$ expressing the WT, the VUS (M192T, S196N, T200K, S206C and T207A) or the mutant S193A were expressed in U2OS cells by transient transfection for 30h before the cells were treated with nocodazole for 14h. Mitotic cells were lysed and immunoprecipitation was performed against the MBP tag using amylose beads. Complexes were resolved on 4-15% SDS-PAGE followed by western blotting using anti-PLK1 and anti-MBP antibodies. StainFree images of the gels before transfer was used as loading control (cropped image is shown). **(B)** Quantification of co-immunoprecipitated PLK1 with 2xMBP-BRCA2$_{1-250}$ in (A), relative to the input levels of PLK1. Results are presented as the fold change compared to BRCA2$_{1-250}$-WT. The data represents the mean ± SD of 2-4 independent experiments (WT (n=4), S193A (n=4), M192T (n=4), S196N (n=4), S206C (n=4), T200K (n=2), T207A (n=3)). Statistical significance of the difference in (b) was calculated with one-way ANOVA test with Tukey's multiple comparisons test. **(C)** PLK1 *in vitro* kinase assay followed by *in vitro* pull-down assay using amylose beads. The polypeptides 2x-MBP-BRCA2$_{1-250}$ WT and T207A were incubated with recombinant PLK1 in the presence of ATP followed by incubation with amylose beads. The bound complexes were eluted from the beads with maltose and resolved on 10% SDS-PAGE followed by western blotting using anti-PLK1 and anti-MBP antibodies. UB: unbound fraction, E: maltose-eluted fraction. **(D)** Quantification of the PLK1 pull-down in (c) relative to the PLK1 levels in the input. Results are presented as the fold change compared to BRCA2$_{1-250}$-WT. The data represents the mean ± SD of three independent experiments. Statistical significance of the difference in (D) was calculated with two-tailed t-test (the p-values show significant differences; ns (non-significant)).

**(E-H)** Isothermal Titration Calorimetry (ITC) thermograms showing binding of $PLK1_{PBD}$ to a 17 aa BRCA2 peptide containing **(E)** pT207, **(F)** T207, **(G)** A207, **(H)** C206pT207. Residues S206 and pT207 are highlighted in pink (S206) and magenta (pT207) in the peptide sequences. **(I)** 3D cartoon representation of the crystal structure of the interface between $PLK1_{PBD}$ (Polo-box 1 in green and Polo-box 2 in blue) and the BRCA2 peptide containing pT207 (in red except for S206 and pT207 that are highlighted in pink and magenta, respectively, as in (Fig. 3E-H)). The left panel shows a global view of the structure, whereas the right panel focuses on the interface between $PLK1_{PBD}$ and the BRCA2 peptide (from A199 to I210, marked in italics). In the left panel, S206 and pT207 are represented in sticks, whereas in the right panel, all the BRCA2 residues observed in the crystal structure are displayed in sticks. The hydrogen bonds involving side chain atoms are displayed and depicted as dark grey dots. The amino acids of $PLK1_{PBD}$ involved in these interactions are highlighted in sticks representation.

**Figure 4. Cells bearing BRCA2 variants S206C and T207A prolong mitosis**

**(A)** Interaction of full-length BRCA2 and PLK1 in stable clones of BRCA2 deficient DLD1 cells ($BRCA2^{-/-}$) expressing EGFPMBP-BRCA2 WT (BRCA2 WT) or the variants S206C or T207A. EGFPMBP-BRCA2 was immunoprecipitated from whole cell lysates of nocadozole treated cells using GFP-trap beads. Immuno-complexes were resolved on 4-15% SDS-PAGE followed by western blotting using anti-BRCA2 and -PLK1 antibodies. Unsynchronized DLD1 cells with endogenous BRCA2 ($BRCA2^{+/+}$) were used as control for the immunoprecipitation and StainFree images of the gels before transfer were used as loading control for the input (cropped image is shown). **(B)** Quantification of co-immunoprecipitated PLK1 with EGFP-MBP-

BRCA2 relative to the PLK1 protein levels in the input. Results are presented as the fold change compared to the EGFPMBP-BRCA2 WT clone. The data represents the mean ± SD of three independent experiments. Statistical significance of the difference was calculated one-way ANOVA test with Tukey's multiple comparisons test.

**(C)** Top: Scheme of the double thymidine block procedure used to synchronize DLD1 cells expressing endogenous BRCA2 ($BRCA2^{+/+}$) or stable clones of DLD1 BRCA2 deficient cells ($BRCA2^{-/-}$) expressing EGFPMBP-BRCA2 WT or VUS, as indicated for live-cell imaging of mitotic progression. Bottom: Representative still images of the live-cell imaging at different time points. The numbers in each image indicate the time in minutes after nuclear envelope break down (NEBD). Scale bar represents 10 µm. **(D)** Frequency distribution of the time cells spend in mitosis from NEBD to daughter cell separation monitored by time-lapse microscopy. The error bars represent SD from at least two-four independent experiments ($BRCA2^{+/+}$ (n=2), $BRCA2^{-/-}$ (n=3), WT C1 (n=5), S206C A7 (n=3), T207A B1 (n=3)), the *n* indicates total number of cells counted. **(E)** Top: Scheme of the double thymidine block procedure used to synchronize DLD1 stable clones for live-cell imaging of mitotic progression from chromosome condensation to anaphase onset. The DNA was labeled with a live cell DNA fluorophore probe (SiR-DNA, 50 nM) added to the cells 7 hours before the start of the filming. Bottom: Representative still images of the live-cell imaging at different time points. The numbers in each image indicate the time in minutes after chromosome condensation, the arrow indicates the onset of anaphase. Scale bar represents 10 µm. **(F)** Quantification of the time the cells spent from chromosome condensation to anaphase onset. The red lines show the mean time ± SD of three or four independent experiments (as in D) with 50 to 80 cells counted per

experiment. The *n* at the top of the graph indicates total number of cells counted from the independent experiments. Statistical significance of the difference in (D and F) was calculated with two- and one-way ANOVA test respectively, with Tukey's multiple comparisons test. The p-values show significant differences; ns (non-significant).

**Figure 5. Cells expressing BRCA2 variants that alter PLK1 phosphorylation display reduced protein levels of phosphorylated BUBR1 and its interaction with PP2A-B56α resulting in chromosomes misalignment**

**(A, B)** Western blots showing the expression levels of endogenous BUBR1 and (A) pT680-BUBR1 or (B) pS676-BUBR1 in nocodazole treated or untreated DLD1 cells expressing endogenous BRCA2 ($BRCA2^{+/+}$) or stable clones of DLD1 BRCA2 deficient cells ($BRCA2^{-/-}$) expressing EGFPMBP-BRCA2 WT (BRCA2 WT) or VUS, as indicated. StainFree image of the gel before transfer is used as loading control (cropped image is shown). **(C)** Co-immunoprecipitation of the tetrameric-protein complex BRCA2-pBUBR1-(PP2A-B56α**)**-PLK1 from mitotic cell extracts of BRCA2 WT cells or cells expressing the variant S206C and T207A using GFP-trap beads. The immuno-complexes were resolved on 4-15% SDS-PAGE followed by western blotting, the interactions were revealed by anti-BRCA2, -pT680-BUBR1, -PLK1 and -PP2AC (PP2A catalytic subunit) antibodies. Mitotic DLD1 cells with endogenous BRCA2 ($BRCA2^{+/+}$) were used as control for the immunoprecipitation and StainFree images of the gels before transfer were used as loading control for the input (cropped image is shown). **(D)** Quantification of co-immunoprecipitated pBUBR1, PLK1 and PP2A with EGFPMBP-BRCA2 in (c), relative to the input levels of each protein. Results are presented as the fold change compared to the BRCA2 WT clone. The

data represents the mean ± SD of three independent experiments. Statistical significance of the difference was calculated two-way ANOVA test with Tukey's multiple comparisons test.

**(E)** Top: Scheme of the double thymidine block procedure used to synchronize the DLD1 cells for analysis of chromosome alignment. Bottom: Quantification of misaligned chromosomes outside the metaphase plate in DLD1 BRCA2 deficient cells expressing BRCA2 WT or S206C and T207A variants. **(F)** Representative images of the type of chromosome alignment observed in cells quantified in (E), scale bar represents 10 µm. Statistical significance of the difference in (E) was calculated with two-way ANOVA test with Tukey's multiple comparisons test (the p-values show differences compared to WT; ns (non-significant)). *n* in (E) indicates the total number of cells counted in each cell line from 2-3 independent experiments.

**Figure 6. Cells expressing BRCA2 VUS S206C and T207A show weaken SAC activity upon nocodazole treatment and display aberrant chromosome segregation**

**(A)** SAC activity was measured by flow cytometry analysis of p-histone 3 expression in DLD1 BRCA2$^{-/-}$ stable clones after treatment with nocodazole for 14h (BRCA2$^{+/+}$ (n=3), BRCA2$^{-/-}$ (n=7), BRCA2 WT (n=7), S206C A7 (n=6) and A9 (n=4), T207A B1 (n=5) and E4 (n=5). **(B)** Top: Scheme of the double thymidine block procedure used to synchronize DLD1 BRCA2$^{-/-}$ stable clones for analysis of aberrant chromosome segregation. Bottom: Quantification of cells with aberrant chromosomes segregation in the stable cells expressing BRCA2 WT, S206C and T207A, as indicated. Statistical significance of the difference in (A) and (B) was calculated with two-way ANOVA test with Tukey's multiple comparisons test (the p-values show the significant differences

compared to WT; ns (non-significant)). *n* in (B) indicates the number of cells counted in each cell clone from a total of 2-4 independent experiments. **(C)** Representative images of the type of aberrant chromosome segregation observed in the cells quantified in (B), CREST antibody is used as marker of centromere; nuclei are revealed with DAPI counterstaining. Scale bars represents 10 µm.

**Figure 7. Cells expressing BRCA2 VUS S206C and T207A exhibit aneuploidy**

**(A)** Distribution of the number of chromosomes observed in metaphase spreads of stable clones expressing BRCA2 WT, S206C A7 or T207 B1 from two independent experiments (total number of cells counted; BRCA2 WT (n=105), S206C A7 (n=111) and T207A B1 (n=110)); modal number of chromosomes and percentage deviating from the mode are shown at the top; p-values were calculated by Mann-Whitney two-tailed test). The cell passage was between 5 and 9 (BRCA2 WT (p.6 and p.9), S206C A7 (p5 and p9) and T207A B1 (p.6 and p.9). **(B)** Representative image of metaphase spreads of the DLD1 BRCA2 deficient stable cells bearing the S206C BRCA2 variant stained with CREST and counterstained with DAPI. In this example, the cell contains 45 chromosomes. **(C-D)** Analysis of S-phase tetraploid cells in DLD1 BRCA2 deficient cells expressing BRCA2 WT or the VUS S206C and T207A measured by flow cytometry after 20 minutes of BrdU incorporation. **(C)** Representative flow cytometry plots of cells stained with anti-BrdU-APC antibodies and 7-AAD (DNA). **(D).** Frequency of S-phase tetraploid cells in stable clones expressing BRCA2 WT or the VUS S206C and T207A. The data represents the mean ± SD of three independent experiments (cell passage: 6-10). Statistical significance of the difference was calculated with one-way ANOVA test with Tukey's multiple comparisons test (the p-values show the difference compared to WT, ns: non-significant).

**Figure 8**. **The DNA repair proficiency is not affected in cells bearing BRCA2 variants S206C and T207A**

**(A)** Quantification of the surviving fraction of DLD1 cells expressing endogenous BRCA2 ($BRCA2^{+/+}$) or stable clones of BRCA2 deficient DLD1 cells ($BRCA2^{-/-}$) expressing BRCA2 WT or the variants S206C or T207A assessed by clonogenic survival upon exposure to MMC at concentrations: 0, 0.5, 1.0 and 2.5 µM. Data are represented as mean ± SD: $BRCA2^{+/+}$ (red) (n=3), $BRCA2^{-/-}$ (gray) (n=5), WT C1 (black) (n=5), S206C A7 (blue) (n=2), T207A B1 (green) (n=4). **(B-C)** Quantification of the relative cell viability monitored by MTT assay upon treatment with increasing doses of MMC (b) or the PARP inhibitor Olaparib (C), as indicated. The data represents the mean ± SD of four (B) and three (C) independent experiments. Statistical significance of the difference in (A-C) was calculated with two-way ANOVA test with Tukey's multiple comparisons test (the p-values show the significant differences compared to the BRCA2 WT clone).

**(D)** Quantification of the percentage of nuclei containing more than 10 γH2AX foci in the indicated cell lines two hours after 6Gy of γ-irradiation (+IR) versus non-irradiated conditions. The data represents the mean ± SD of three to four independent experiments; the *n* at the top of the graph indicates total number of cells counted. **(E)** Boxplot quantification of a representative experiment showing the ratio of RAD51/γH2AX foci per nucleus in the same cells and conditions as quantified in (D). Boxes represent the 25-75% percentiles, the whiskers the 5-95% percentiles and the median is indicated with a horizontal line. The *n* at the top of the graph indicates number of cells counted in the experiment, in total two to three independent experiments were performed with at least 300 cells counted per cell clone and condition. Statistical significance of the difference in (D-E) was calculated with

unpaired two-tailed t-test (the p-values show the significant difference, ns: non-significant). **(F)** Model for the role of PLK1 phosphorylation of BRCA2 in mitosis (see text for details). In panels 2, 2', 3 and 3' blue blobs represent chromosomes, red circles represent the kinetochores, red cylinders represent the centrioles and orange lanes represent the spindle microtubules.

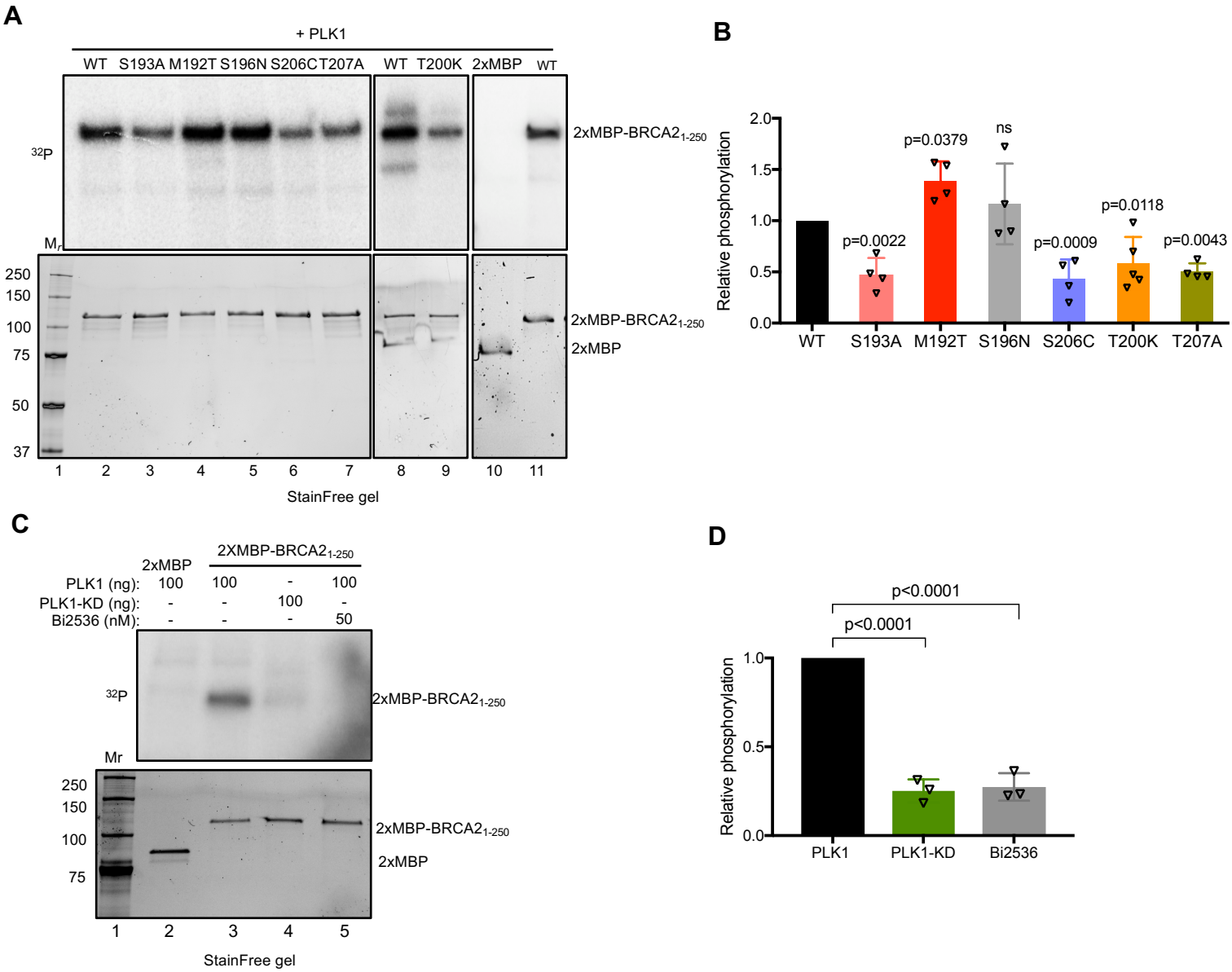
A
+ PLK1
WT S193A M192T S196N S206C T207A WT T200K 2xMBP WT
32P
2xMBP-BRCA2 1-250
Mr
250
150
100
75
50
37
2xMBP-BRCA2 1-250
2xMBP
1 2 3 4 5 6 7 8 9 10 11
StainFree gel
B
Relative phosphorylation
2.0
1.5
1.0
0.5
0.0
p=0.0022
p=0.0379
ns
p=0.0009
p=0.0118
p=0.0043
WT S193A M192T S196N S206C T200K T207A
C
2xMBP
2XMBP-BRCA2 1-250
PLK1 (ng): 100 100 - 100
PLK1-KD (ng): - - 100 -
Bi2536 (nM): - - - 50
32P
2xMBP-BRCA2 1-250
Mr
250
150
100
75
2xMBP-BRCA2 1-250
2xMBP
1 2 3 4 5
StainFree gel
D
p<0.0001
p<0.0001
Relative phosphorylation
1.0
0.5
0.0
PLK1 PLK1-KD Bi2536

Figure 1

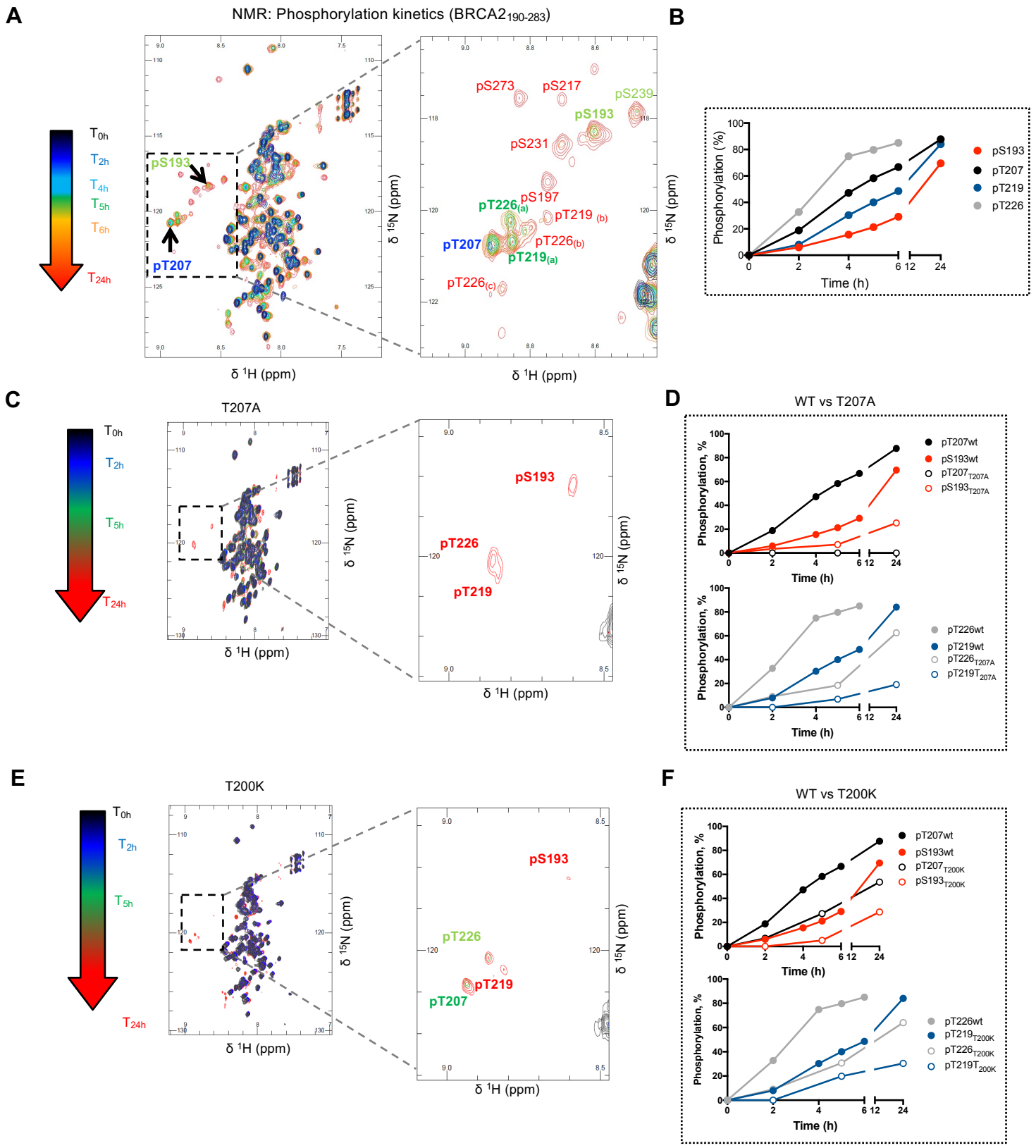
A
NMR: Phosphorylation kinetics (BRCA2190-283)
T0h
T2h
T4h
T5h
T6h
T24h
pS193
pT207
δ 1H (ppm)
δ 15N (ppm)
pS273
pS217
pS239
pS193
pS231
pS197
pT226(a)
pT219 (b)
pT207
pT226(b)
pT219(a)
pT226(c)
B
Phosphorylation (%)
Time (h)
pS193
pT207
pT219
pT226
C
T207A
pS193
pT226
pT219
D
WT vs T207A
Phosphorylation, %
Time (h)
pT207wt
pS193wt
pT207T207A
pS193T207A
pT226wt
pT219wt
pT226T207A
pT219T207A
E
T200K
pS193
pT226
pT219
pT207
F
WT vs T200K
pT207wt
pS193wt
pT207T200K
pS193T200K
pT226wt
pT219T200K
pT226T200K
pT219T200K

Figure 2

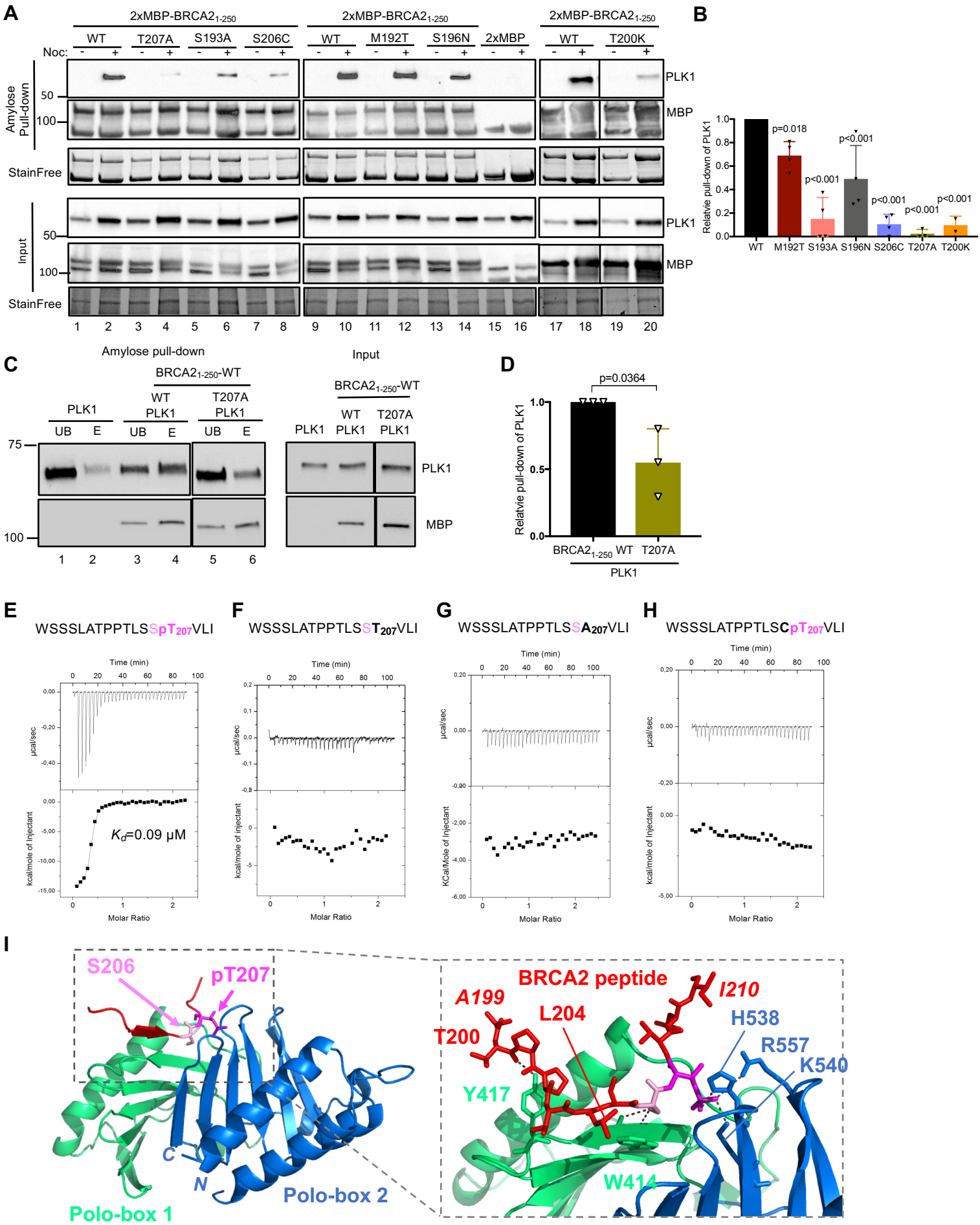
A
2xMBP-BRCA2$_{1-250}$
WT
T207A
S193A
S206C
M192T
S196N
2xMBP
T200K
Noc:
Amylose Pull-down
Input
PLK1
MBP
StainFree
B
Relatvie pull-down of PLK1
p=0.018
p<0.001
WT
M192T
S193A
S196N
S206C
T207A
T200K
C
Amylose pull-down
Input
BRCA2$_{1-250}$-WT
UB
E
D
p=0.0364
Relatvie pull-down of PLK1
BRCA2$_{1-250}$
E
WSSSLATPPTLSSpT$_{207}$VLI
F
WSSSLATPPTLSST$_{207}$VLI
G
WSSSLATPPTLSSA$_{207}$VLI
H
WSSSLATPPTLSCpT$_{207}$VLI
Time (min)
µcal/sec
kcal/mole of Injectant
Molar Ratio
$K_d$=0.09 µM
I
S206
pT207
BRCA2 peptide
A199
L204
I210
T200
H538
R557
K540
Y417
W414
C
N
Polo-box 1
Polo-box 2

Figure 3

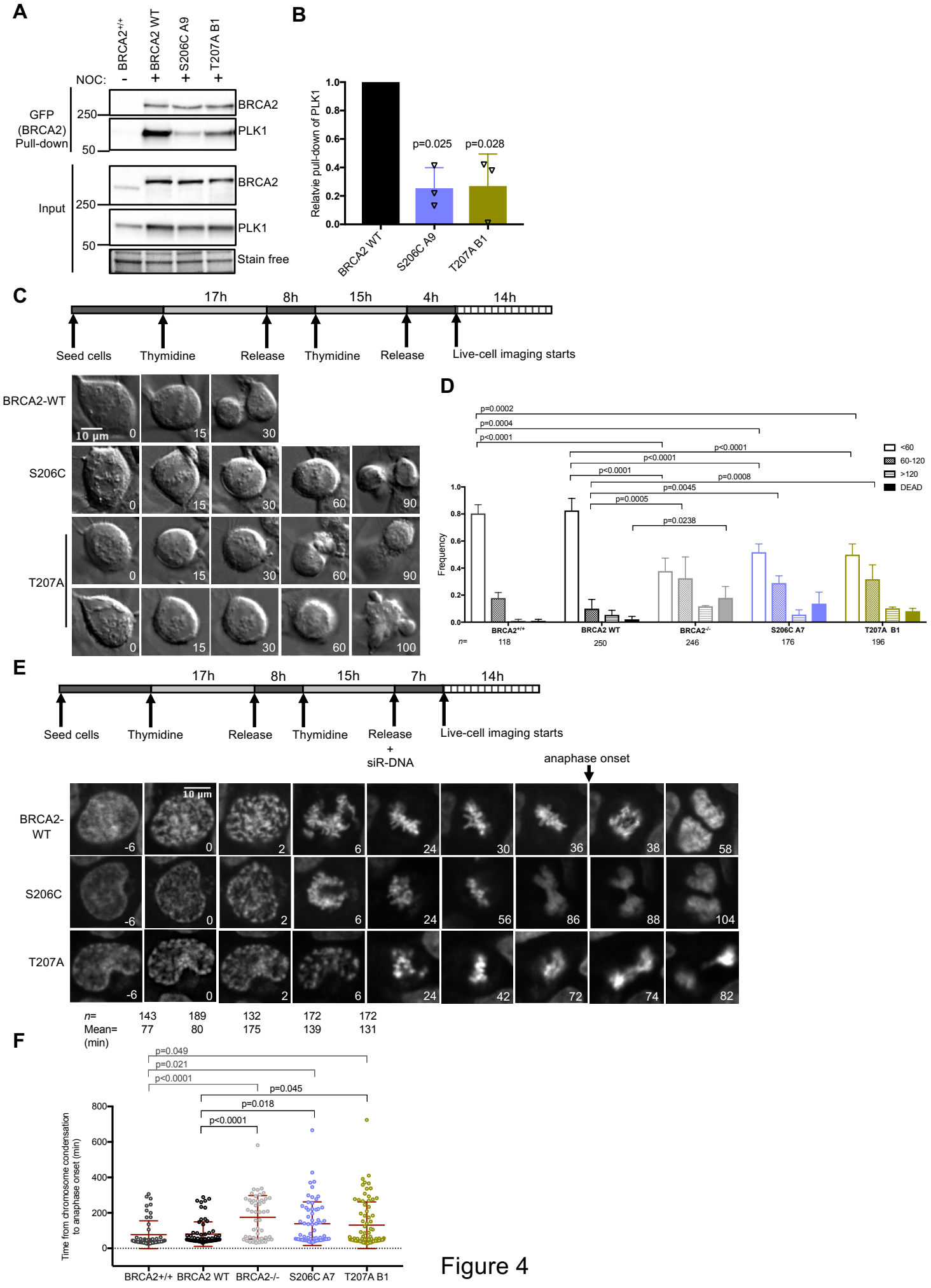
A
NOC:
- BRCA2+/+
+ BRCA2 WT
+ S206C A9
+ T207A B1
GFP (BRCA2) Pull-down
250
50
BRCA2
PLK1
Input
250
50
BRCA2
PLK1
Stain free
B
Relatvie pull-down of PLK1
1.0
0.8
0.6
0.4
0.2
0.0
p=0.025
p=0.028
BRCA2 WT
S206C A9
T207A B1
C
17h
8h
15h
4h
14h
Seed cells
Thymidine
Release
Thymidine
Release
Live-cell imaging starts
BRCA2-WT
S206C
T207A
10 µm
0
15
30
60
90
100
D
p=0.0002
p=0.0004
p<0.0001
p<0.0001
p<0.0001
p<0.0001
p=0.0008
p=0.0045
p=0.0005
p=0.0238
<60
60-120
>120
DEAD
Frequency
BRCA2+/+
BRCA2 WT
BRCA2-/-
S206C A7
T207A B1
n=
118
250
246
176
196
E
17h
8h
15h
7h
14h
Seed cells
Thymidine
Release
Thymidine
Release + siR-DNA
Live-cell imaging starts
anaphase onset
BRCA2-WT
S206C
T207A
10 µm
-6
0
2
6
24
30
36
38
58
56
86
88
104
42
72
74
82
n=
143
189
132
172
172
Mean= (min)
77
80
175
139
131
F
p=0.049
p=0.021
p<0.0001
p=0.045
p=0.018
p<0.0001
Time from chromosome condensation to anaphase onset (min)
800
600
400
200
0
BRCA2+/+
BRCA2 WT
BRCA2-/-
S206C A7
T207A B1

Figure 4

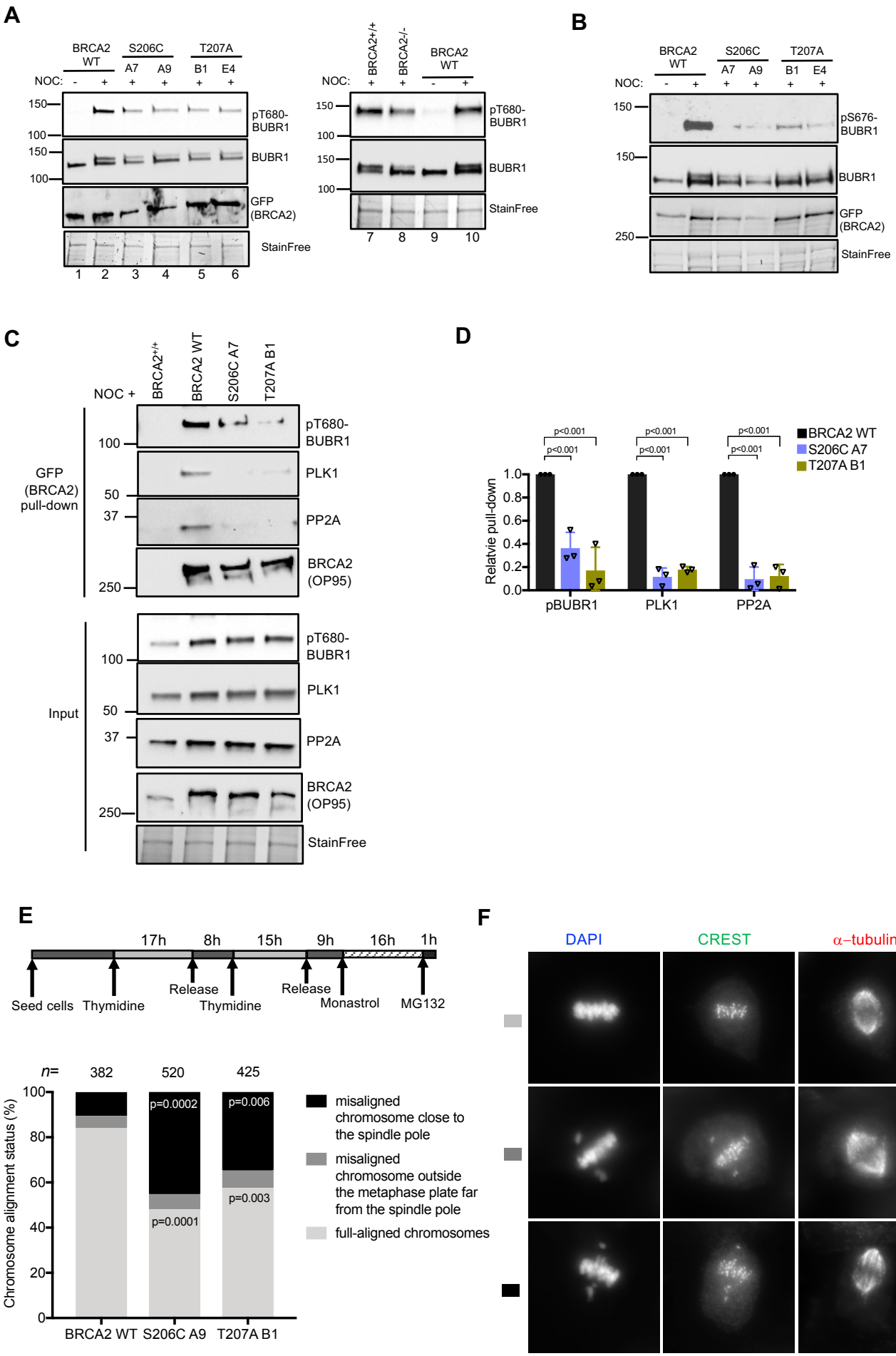
A
BRCA2 WT
S206C
T207A
A7
A9
B1
E4
NOC:
pT680-BUBR1
BUBR1
GFP (BRCA2)
StainFree
BRCA2+/+
BRCA2-/-
B
pS676-BUBR1
C
GFP (BRCA2) pull-down
Input
PLK1
PP2A
BRCA2 (OP95)
D
Relatvie pull-down
pBUBR1
p<0.001
E
17h
8h
15h
9h
16h
1h
Seed cells
Thymidine
Release
Monastrol
MG132
n=
382
520
425
Chromosome alignment status (%)
p=0.0002
p=0.0001
p=0.006
p=0.003
misaligned chromosome close to the spindle pole
misaligned chromosome outside the metaphase plate far from the spindle pole
full-aligned chromosomes
F
DAPI
CREST
α–tubulin
MERGE
10 µm

Figure 5

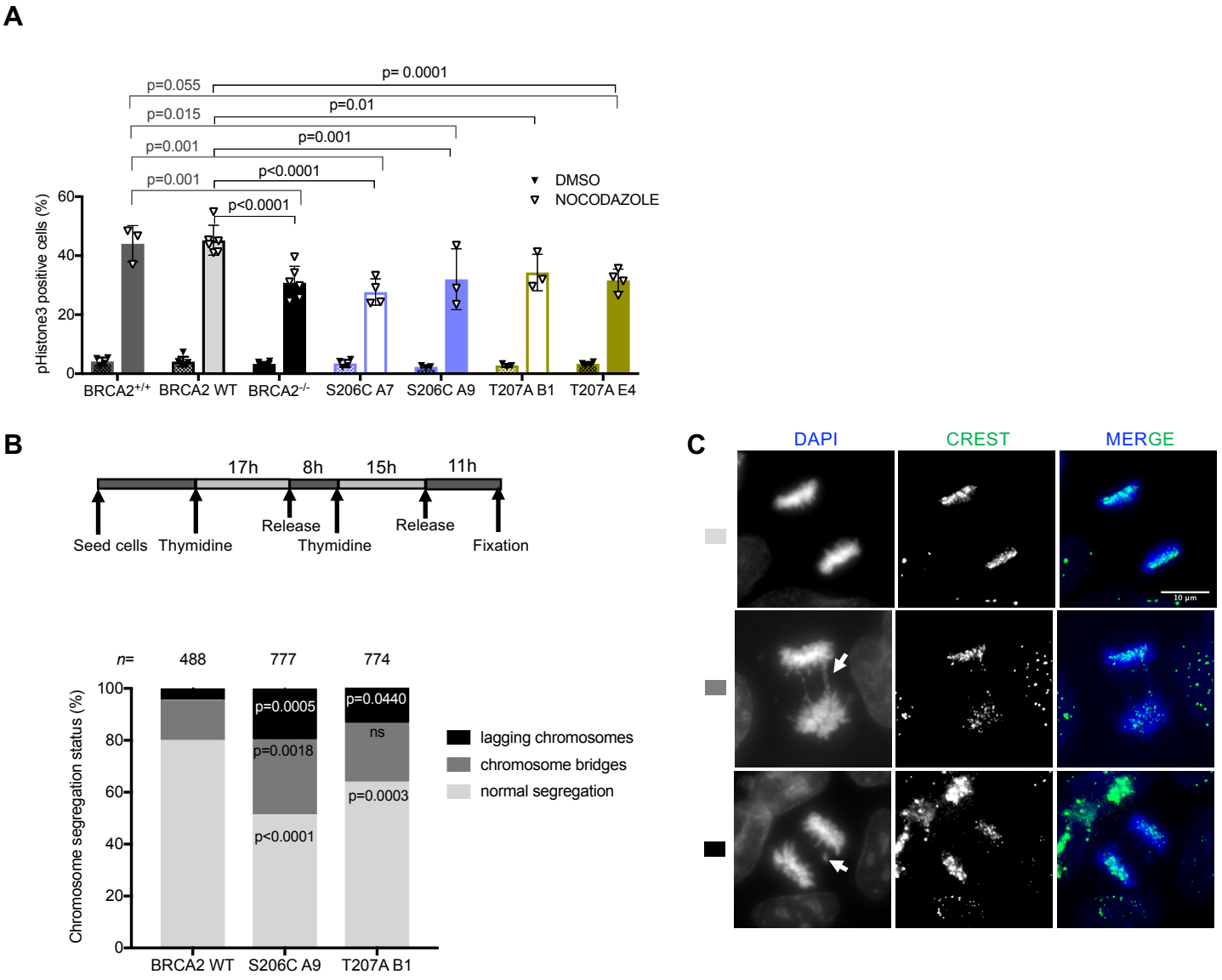
A
p= 0.0001
p=0.055
p=0.01
p=0.015
p=0.001
p=0.001
p<0.0001
p=0.001
p<0.0001
DMSO
NOCODAZOLE
pHistone3 positive cells (%)
60
40
20
0
BRCA2+/+
BRCA2 WT
BRCA2-/-
S206C A7
S206C A9
T207A B1
T207A E4
B
17h
8h
15h
11h
Seed cells
Thymidine
Release
Thymidine
Release
Fixation
n=
488
777
774
Chromosome segregation status (%)
100
80
60
40
20
0
p=0.0005
p=0.0018
p<0.0001
p=0.0440
ns
p=0.0003
lagging chromosomes
chromosome bridges
normal segregation
BRCA2 WT
S206C A9
T207A B1
C
DAPI
CREST
MERGE
10 µm

Figure 6

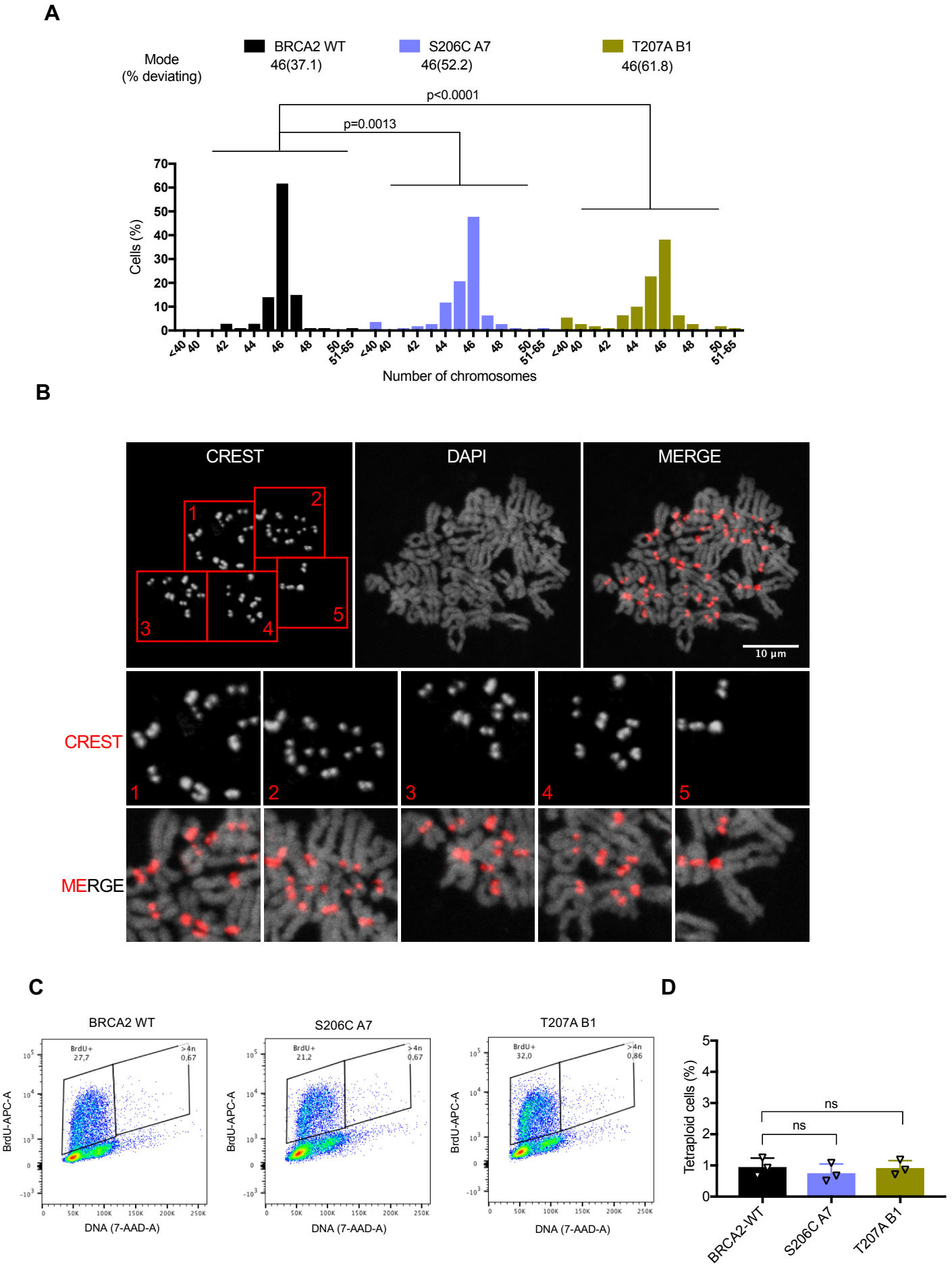
A
Mode
(% deviating)
BRCA2 WT
46(37.1)
S206C A7
46(52.2)
T207A B1
46(61.8)
p<0.0001
p=0.0013
Cells (%)
Number of chromosomes
B
CREST
DAPI
MERGE
10 µm
CREST
MERGE
C
BRCA2 WT
S206C A7
T207A B1
BrdU-APC-A
DNA (7-AAD-A)
D
Tetraploid cells (%)
ns
ns
BRCA2-WT
S206C A7
T207A B1

Figure 7

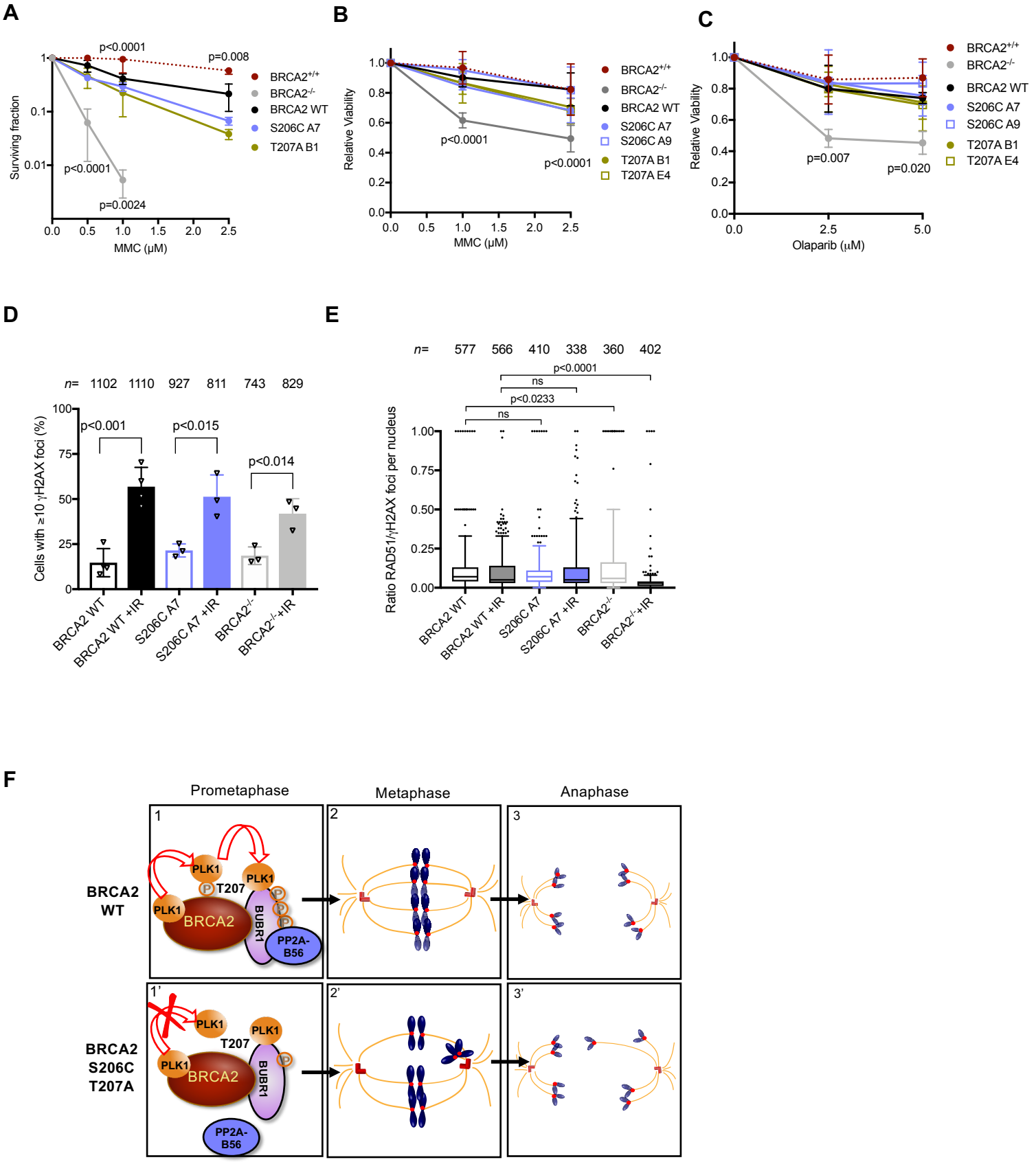
A
Surviving fraction
MMC (μM)
p<0.0001
p=0.008
p<0.0001
p=0.0024
BRCA2+/+
BRCA2-/-
BRCA2 WT
S206C A7
T207A B1
B
Relative Viability
MMC (μM)
p<0.0001
p<0.0001
BRCA2+/+
BRCA2-/-
BRCA2 WT
S206C A7
S206C A9
T207A B1
T207A E4
C
Relative Viability
Olaparib (μM)
p=0.007
p=0.020
BRCA2+/+
BRCA2-/-
BRCA2 WT
S206C A7
S206C A9
T207A B1
T207A E4
D
n= 1102 1110 927 811 743 829
Cells with ≥10 γH2AX foci (%)
p<0.001
p<0.015
p<0.014
BRCA2 WT
BRCA2 WT +IR
S206C A7
S206C A7 +IR
BRCA2-/-
BRCA2-/-+IR
E
n= 577 566 410 338 360 402
Ratio RAD51/γH2AX foci per nucleus
p<0.0001
ns
p<0.0233
ns
BRCA2 WT
BRCA2 WT +IR
S206C A7
S206C A7 +IR
BRCA2-/-
BRCA2-/-+IR
F
Prometaphase
Metaphase
Anaphase
BRCA2 WT
BRCA2 S206C T207A
PLK1
T207
BRCA2
BUBR1
PP2A-B56
1
2
3
1'
2'
3'

Figure 8

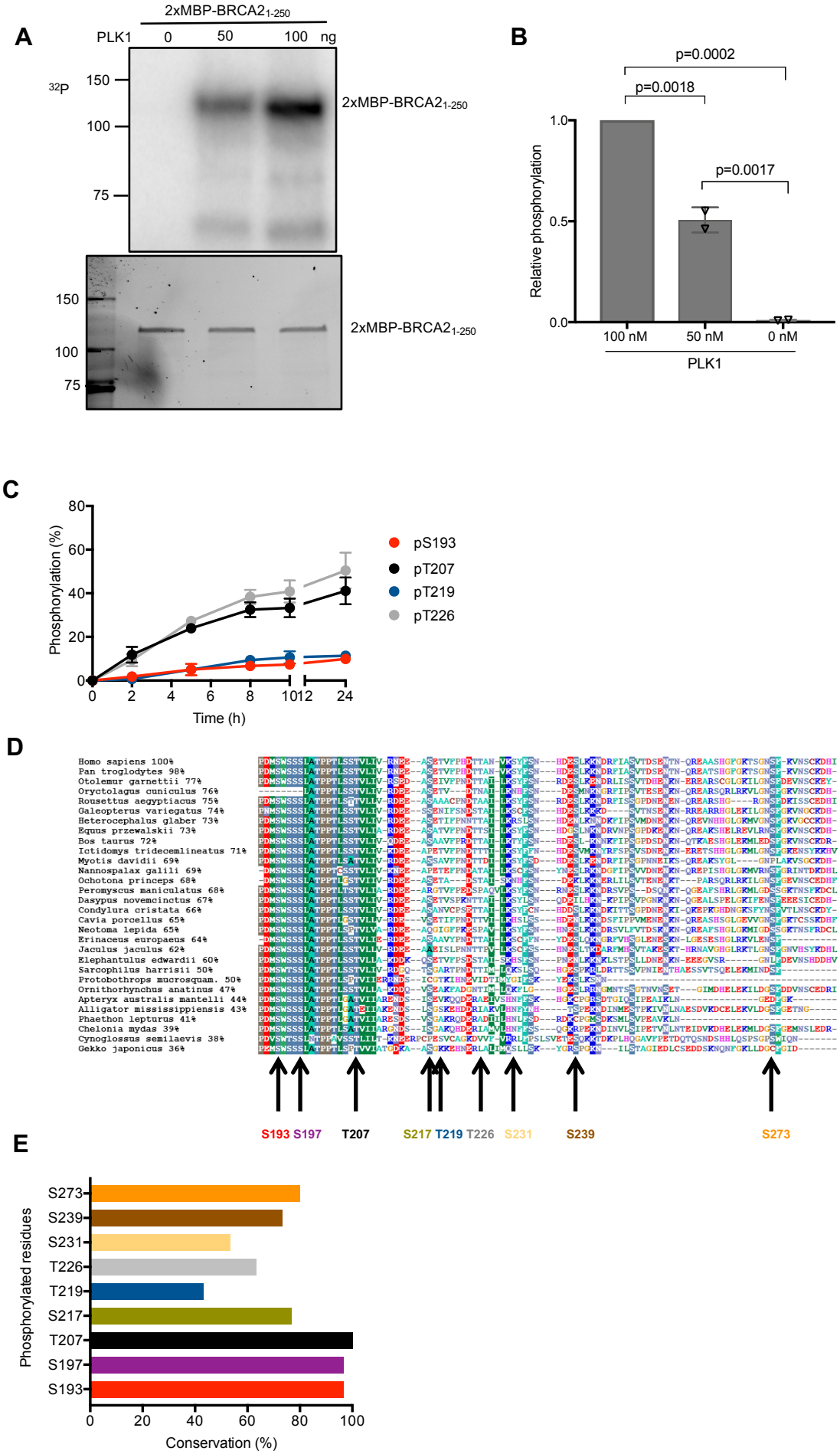
A
2xMBP-BRCA2$_{1-250}$
PLK1
0
50
100
ng
$^{32}$P
150
100
75
2xMBP-BRCA2$_{1-250}$
150
100
75
2xMBP-BRCA2$_{1-250}$
B
p=0.0002
p=0.0018
p=0.0017
Relative phosphorylation
1.0
0.5
0.0
100 nM
50 nM
0 nM
PLK1
C
Phosphorylation (%)
80
60
40
20
0
0
2
4
6
8
10
12
24
Time (h)
pS193
pT207
pT219
pT226
D
Homo sapiens 100%
Pan troglodytes 98%
Otolemur garnettii 77%
Oryctolagus cuniculus 76%
Rousettus aegyptiacus 75%
Galeopterus variegatus 74%
Heterocephalus glaber 73%
Equus przewalskii 73%
Bos taurus 72%
Ictidomys tridecemlineatus 71%
Myotis davidii 69%
Nannospalax galili 69%
Ochotona princeps 68%
Peromyscus maniculatus 68%
Dasypus novemcinctus 67%
Condylura cristata 66%
Cavia porcellus 65%
Neotoma lepida 65%
Erinaceus europaeus 64%
Jaculus jaculus 62%
Elephantulus edwardii 60%
Sarcophilus harrisii 50%
Protobothrops mucrosquam. 50%
Ornithorhynchus anatinus 47%
Apteryx australis mantelli 44%
Alligator mississippiensis 43%
Phaethon lepturus 41%
Chelonia mydas 39%
Cynoglossus semilaevis 38%
Gekko japonicus 36%
S193 S197
T207
S217 T219 T226
S231
S239
S273
E
Phosphorylated residues
S273
S239
S231
T226
T219
S217
T207
S197
S193
0
20
40
60
80
100
Conservation (%)

Figure S1

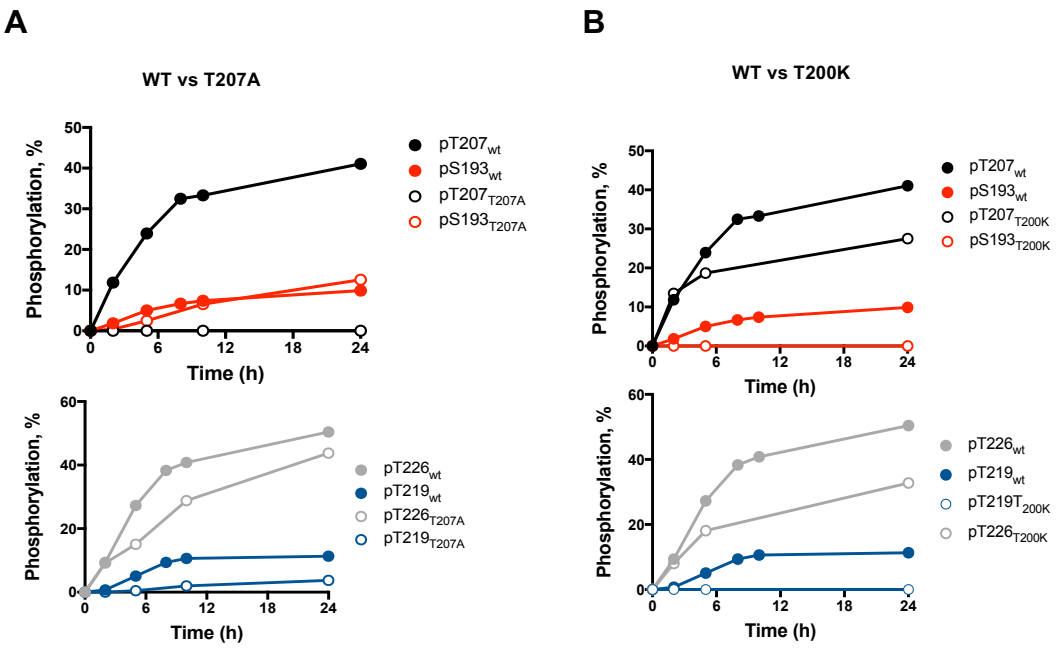
A
WT vs T207A
Phosphorylation, %
Time (h)
pT207wt
pS193wt
pT207T207A
pS193T207A
pT226wt
pT219wt
pT226T207A
pT219T207A
B
WT vs T200K
Phosphorylation, %
Time (h)
pT207wt
pS193wt
pT207T200K
pS193T200K
pT226wt
pT219wt
pT219T200K
pT226T200K

Figure S2

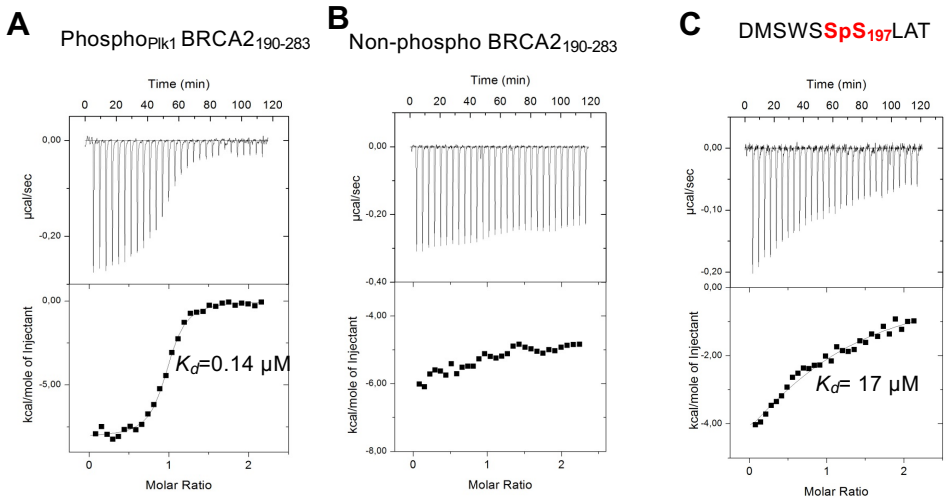
A
Phospho$_{Plk1}$ BRCA2$_{190-283}$
B
Non-phospho BRCA2$_{190-283}$
C
DMSWSSpS$_{197}$LAT
Time (min)
µcal/sec
kcal/mole of Injectant
Molar Ratio
$K_d$=0.14 µM
$K_d$= 17 µM

Figure S3

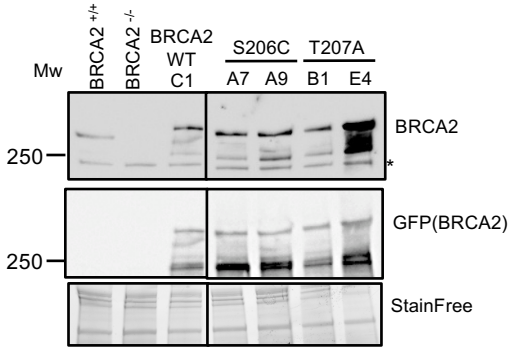
Mw
BRCA2 +/+
BRCA2 -/-
BRCA2 WT C1
S206C
T207A
A7
A9
B1
E4
250
BRCA2
*
250
GFP(BRCA2)
StainFree

Figure S4

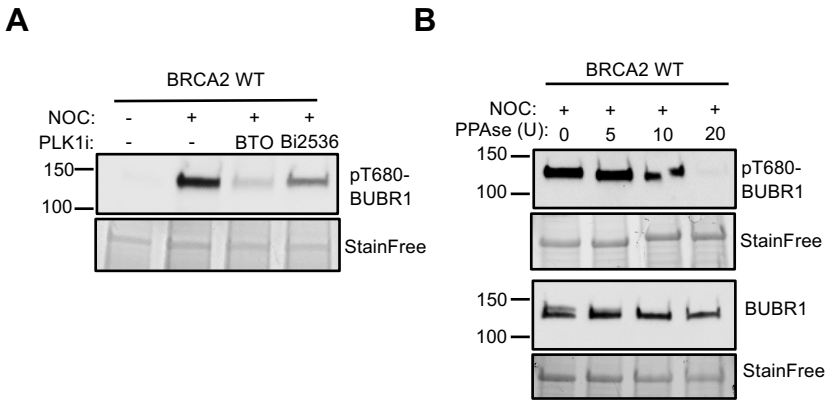
A
BRCA2 WT
NOC: - + + +
PLK1i: - - BTO Bi2536
150
100
pT680-
BUBR1
StainFree
B
BRCA2 WT
NOC: + + + +
PPAse (U): 0 5 10 20
150
100
pT680-
BUBR1
StainFree
150
100
BUBR1
StainFree

Figure S5

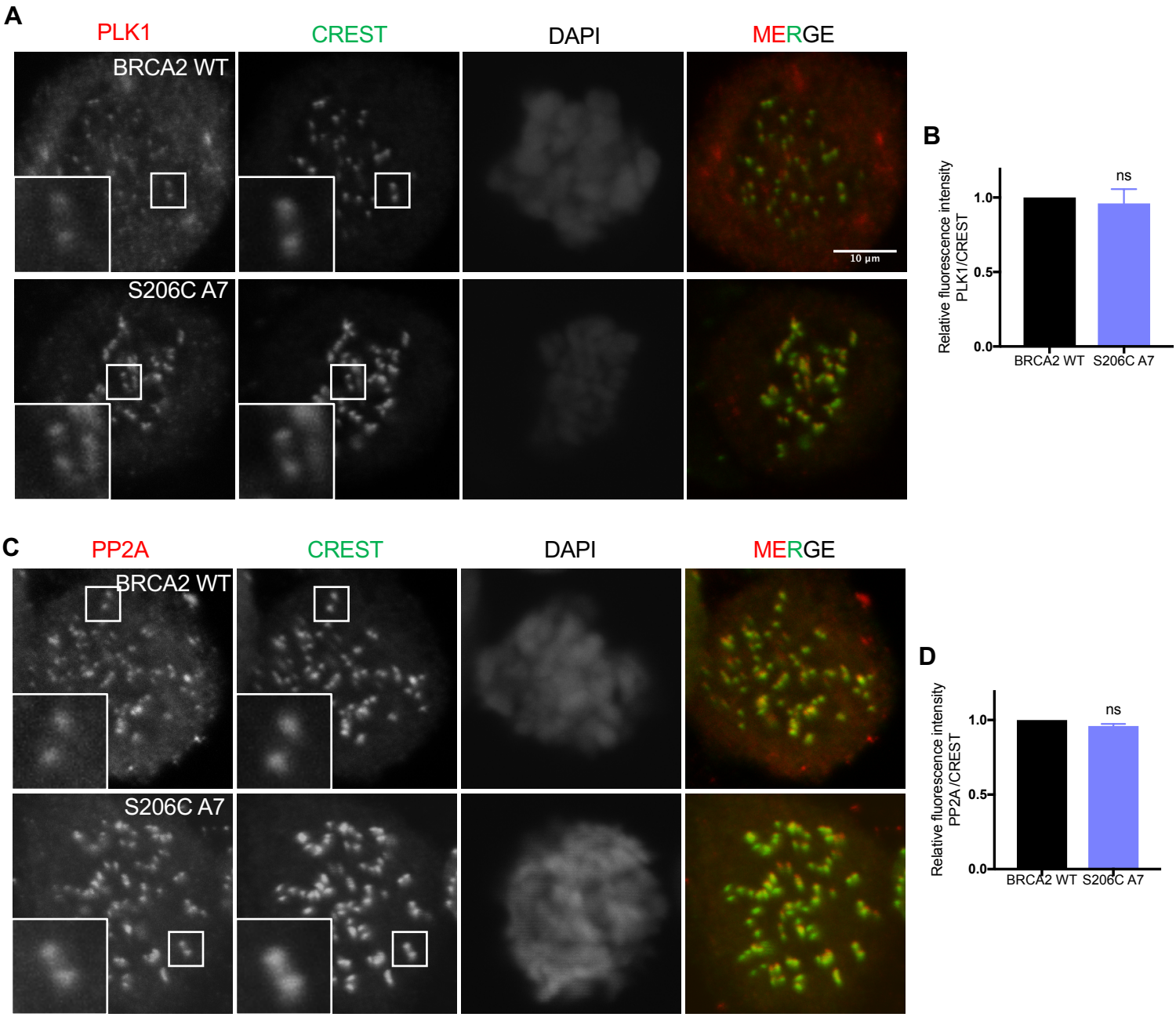
A
PLK1
CREST
DAPI
MERGE
BRCA2 WT
S206C A7
10 µm
B
Relative fluorescence intensity
PLK1/CREST
ns
1.0
0.5
0.0
BRCA2 WT
S206C A7
C
PP2A
CREST
DAPI
MERGE
BRCA2 WT
S206C A7
D
Relative fluorescence intensity
PP2A/CREST
ns
1.0
0.5
0.0
BRCA2 WT
S206C A7

Figure S6

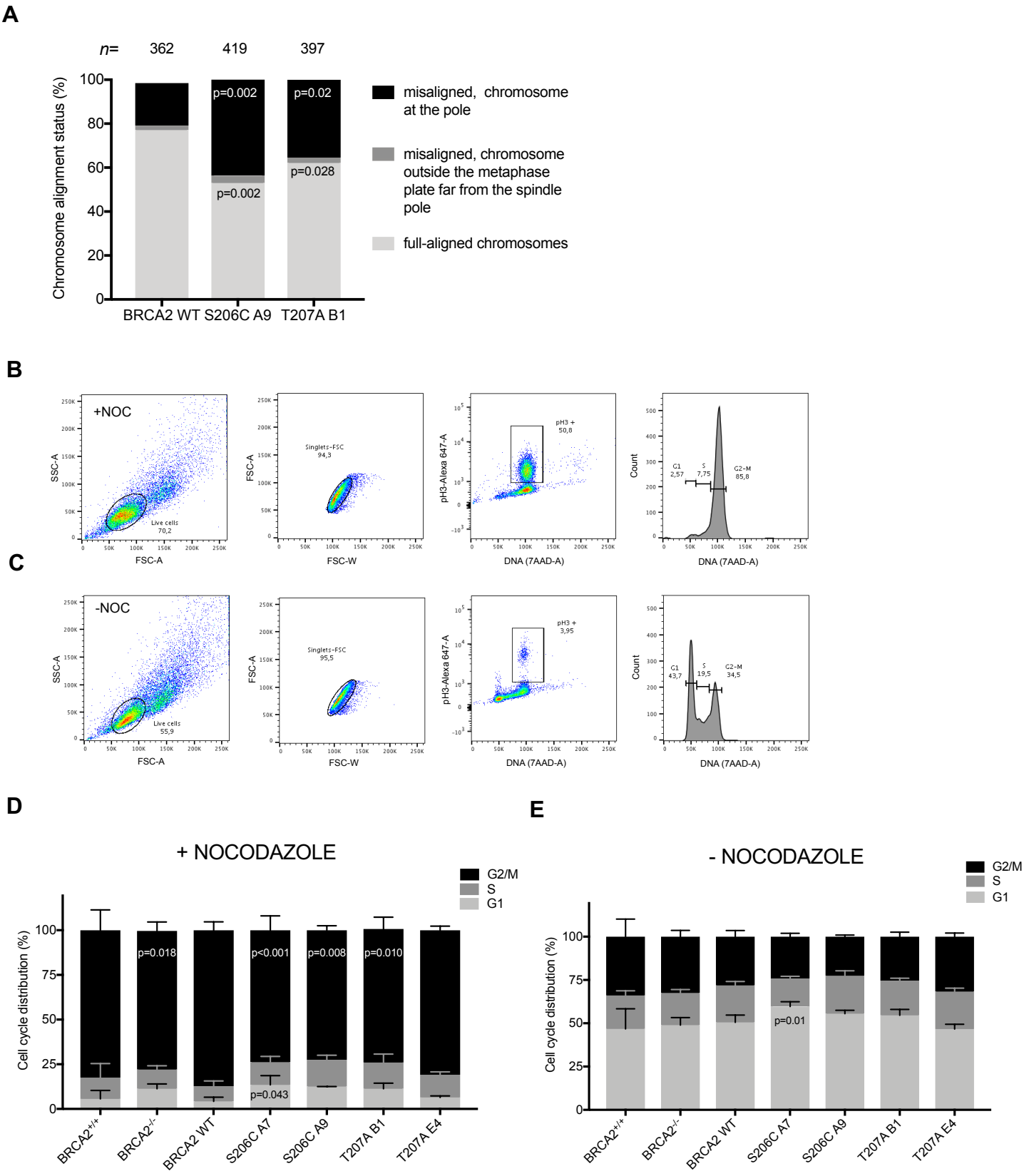
A
n= 362 419 397
Chromosome alignment status (%)
p=0.002
p=0.002
p=0.02
p=0.028
BRCA2 WT S206C A9 T207A B1
misaligned, chromosome at the pole
misaligned, chromosome outside the metaphase plate far from the spindle pole
full-aligned chromosomes
B
+NOC
Live cells 70,2
Singlets-FSC 94,3
pH3 + 50,8
G1 2,57
S 7,75
G2-M 85,8
C
-NOC
Live cells 55,9
Singlets-FSC 95,5
pH3 + 3,95
G1 43,7
S 19,5
G2-M 34,5
SSC-A
FSC-A
FSC-W
pH3-Alexa 647-A
DNA (7AAD-A)
Count
D
+ NOCODAZOLE
Cell cycle distribution (%)
G2/M
S
G1
p=0.018
p<0.001
p=0.008
p=0.010
p=0.043
BRCA2+/+
BRCA2-/-
BRCA2 WT
S206C A7
S206C A9
T207A B1
T207A E4
E
- NOCODAZOLE
p=0.01

Figure S7

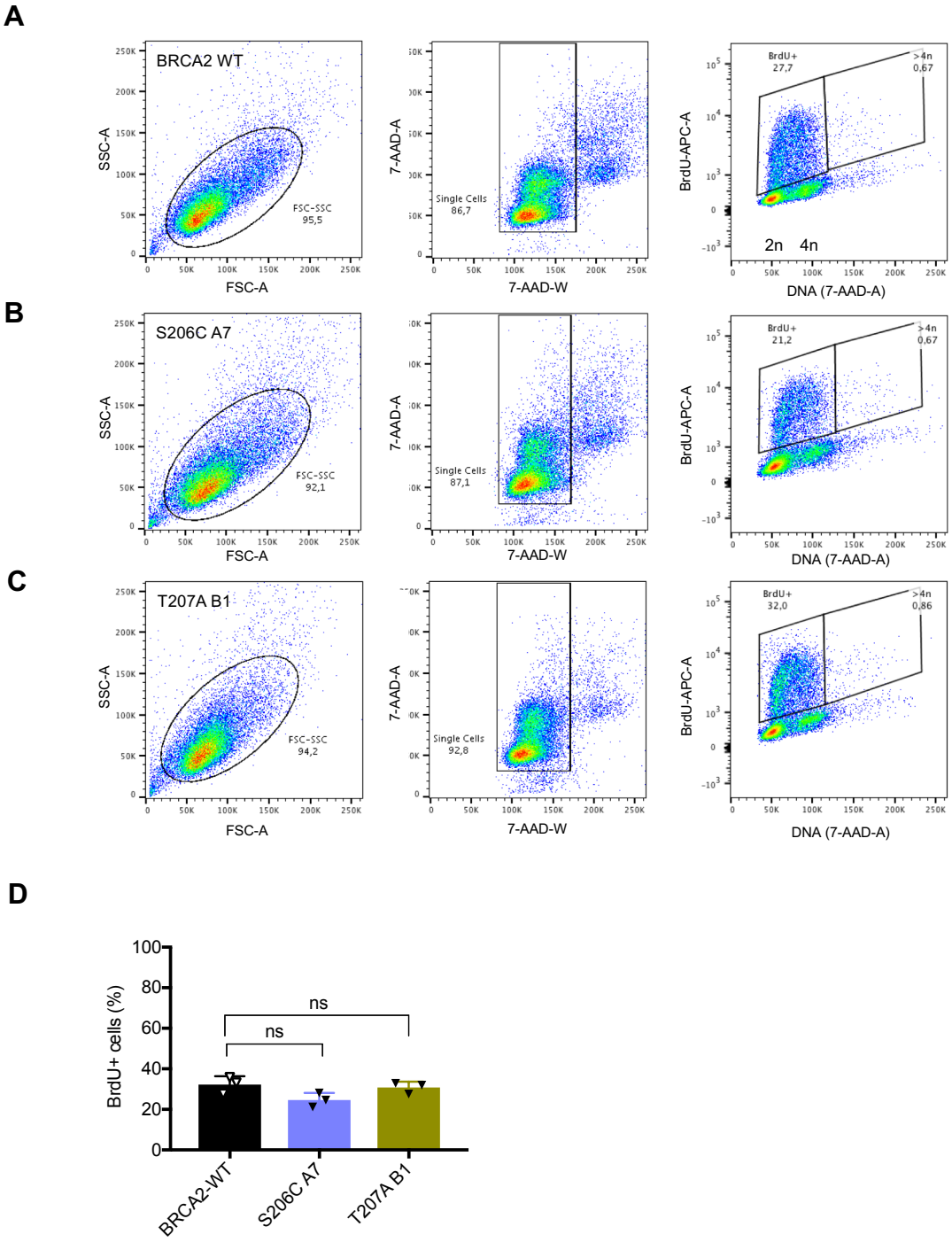
A
BRCA2 WT
SSC-A
FSC-A
FSC-SSC
95,5
7-AAD-A
7-AAD-W
Single Cells
86,7
BrdU-APC-A
DNA (7-AAD-A)
BrdU+
27,7
>4n
0,67
2n
4n
B
S206C A7
FSC-SSC
92,1
Single Cells
87,1
BrdU+
21,2
>4n
0,67
C
T207A B1
FSC-SSC
94,2
Single Cells
92,8
BrdU+
32,0
>4n
0,86
D
BrdU+ cells (%)
ns
ns
BRCA2-WT
S206C A7
T207A B1

Figure S8

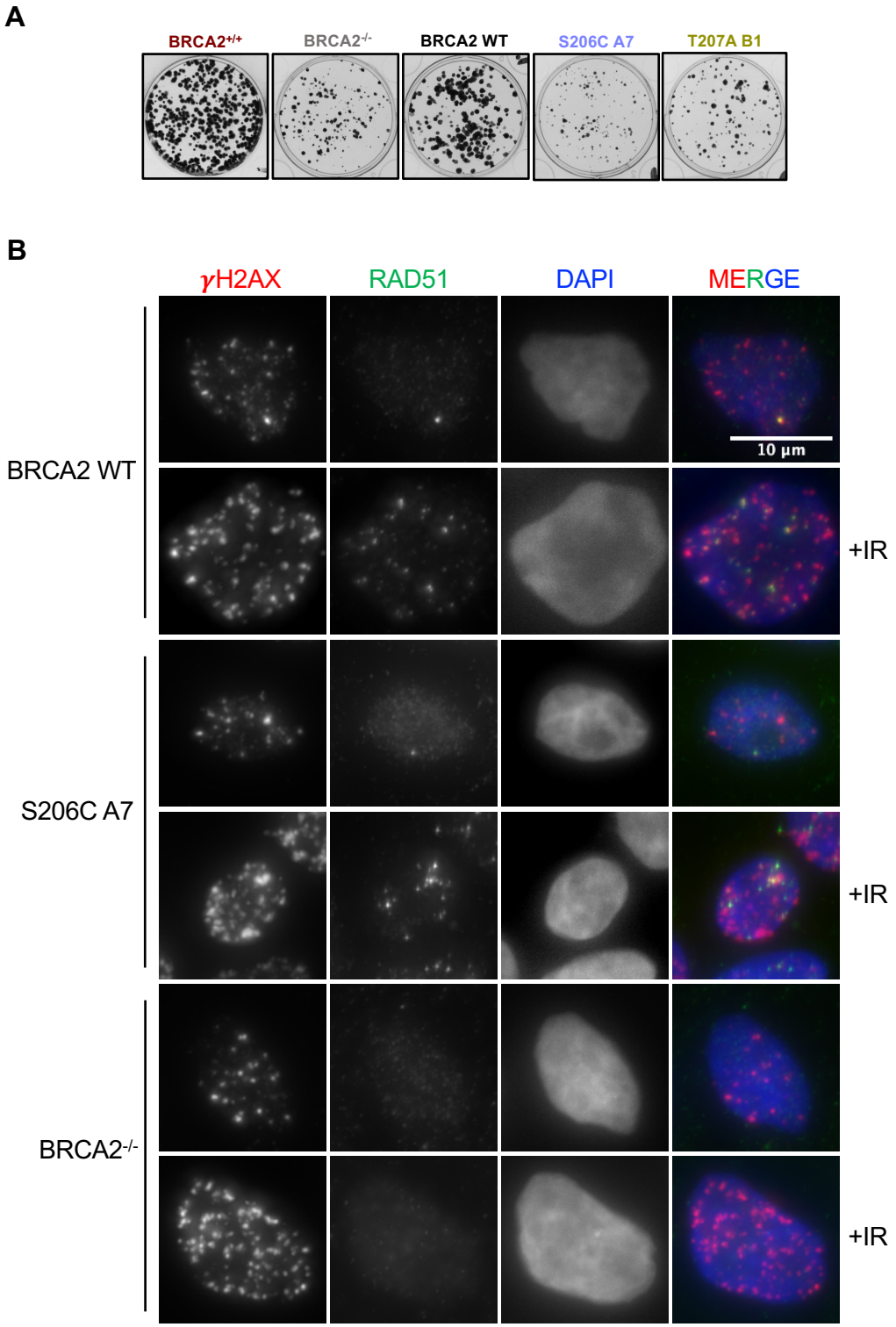
A
BRCA2+/+
BRCA2-/-
BRCA2 WT
S206C A7
T207A B1
B
γH2AX
RAD51
DAPI
MERGE
10 µm
BRCA2 WT
+IR
S206C A7
+IR
BRCA2-/-
+IR

Figure S9

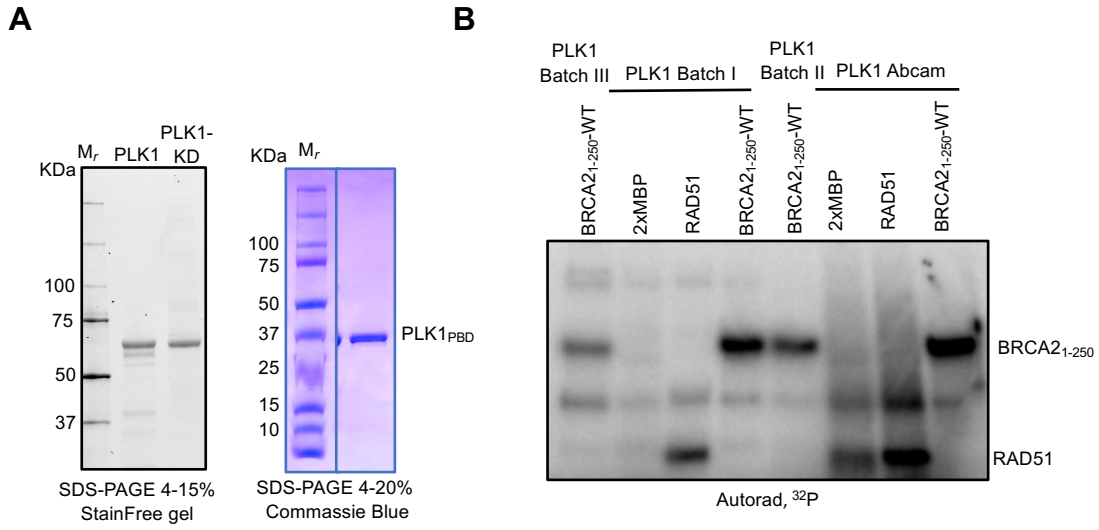
A
B
KDa
Mr
PLK1
PLK1-KD
100
75
50
37
SDS-PAGE 4-15%
StainFree gel
KDa
Mr
100
75
50
37
25
15
10
PLK1PBD
SDS-PAGE 4-20%
Commassie Blue
PLK1 Batch III
PLK1 Batch I
PLK1 Batch II
PLK1 Abcam
BRCA21-250-WT
2xMBP
RAD51
BRCA21-250-WT
BRCA21-250-WT
2xMBP
RAD51
BRCA21-250-WT
BRCA21-250
RAD51
Autorad, 32P

Figure S10